ARL-TR-85-14 Copy No. 14

AN EXPERIMENTAL INVESTIGATION OF ACOUSTIC PROPAGATION IN SATURATED SANDS WITH VARIABLE FLUID PROPERTIES

R. Daniel Costley, Jr.

APPLIED RESEARCH LABORATORIES
THE UNIVERSITY OF TEXAS AT AUSTIN
POST OFFICE BOX 8029, AUSTIN, TEXAS 78713-8029

May 1985

Technical Report

Prepared for:

OFFICE OF NAVAL RESEARCH
DEPARTMENT OF THE NAVY
ARLINGTON, VA 22217

UNCLASSIFIED

SECURITY CLASSIFICATION OF THIS PAGE *(When Data Entered)*

REPORT DOCUMENTATION PAGE		READ INSTRUCTIONS BEFORE COMPLETING FORM
1. REPORT NUMBER	2. GOVT ACCESSION NO. AD-A159 930	3. RECIPIENT'S CATALOG NUMBER
4. TITLE *(and Subtitle)* AN EXPERIMENTAL INVESTIGATION OF ACOUSTIC PROPAGATION IN SATURATED SANDS WITH VARIABLE FLUID PROPERTIES		5. TYPE OF REPORT & PERIOD COVERED
		6. PERFORMING ORG. REPORT NUMBER ARL-TR-85-14
7. AUTHOR(s) R. Daniel Costley, Jr.		8. CONTRACT OR GRANT NUMBER(s) N00014-80-C-0490
9. PERFORMING ORGANIZATION NAME AND ADDRESS Applied Research Laboratories The University of Texas at Austin Austin, Texas 78713-8029		10. PROGRAM ELEMENT, PROJECT, TASK AREA & WORK UNIT NUMBERS technical report
11. CONTROLLING OFFICE NAME AND ADDRESS Office of Naval Research Department of the Navy Arlington, Virginia 22217		12. REPORT DATE May 1985
		13. NUMBER OF PAGES 100
14. MONITORING AGENCY NAME & ADDRESS *(if different from Controlling Office)*		15. SECURITY CLASS. *(of this report)* UNCLASSIFIED
		15a. DECLASSIFICATION/DOWNGRADING SCHEDULE

16. DISTRIBUTION STATEMENT *(of this Report)*

17. DISTRIBUTION STATEMENT *(of the abstract entered in Block 20, if different from Report)*

Approved for public release; distribution unlimited.

18. SUPPLEMENTARY NOTES (cont'd p. 2)

19. KEY WORDS *(Continue on reverse side if necessary and identify by block number)*

compressional velocity; experiment
compressional attenuation; sand
Biot theory;
viscosity dependence.

20. ABSTRACT *(Continue on reverse side if necessary and identify by block number)*

The Biot-Stoll theory describes the propagation of acoustic waves in a saturated, unconsolidated porous medium. The expressions for the attenuation and phase velocity derived from this theory depend explicitly on the viscosity, density, and bulk modulus of the pore fluid. An experiment has been designed to determine the dependence of attenuation and phase velocity on these properties of the pore fluid. The phase velocity and attenuation of compressional waves were measured using a mixture of water and glycerine as the interstitial fluid. The theoretical background is reviewed and the experimental procedure is discussed in

DD FORM 1 JAN 73 1473 EDITION OF 1 NOV 65 IS OBSOLETE

UNCLASSIFIED

SECURITY CLASSIFICATION OF THIS PAGE *(When Data Entered)*

20. (cont'd)

detail. The results, along with comparisons with the Biot-Stoll theory, are then presented. The choices of the theoretical parameters are discussed and their relation to the fit of the theory to the data. The Biot-Stoll theory is shown to adequately describe the effects of the fluid properties on acoustic wave propagation in saturated sediments, at least for compressional waves of the first type. Keywords: Stoll

TABLE OF CONTENTS

LIST OF TABLES

I. INTRODUCTION

There has been continued interest in acoustic propagation in fluid saturated, porous media for the past three decades. Initially, much of the interest was due to problems encountered in the oil industry. Acoustic techniques were devised, and are still being developed and used, to determine the properties of the porous rocks, and their interstitial fluids, found at different depths in oil wells. Maurice Biot, while working for Shell Development Company, published two papers in 1956 and a third in 1962 describing wave propagation in fluid saturated, porous, elastic solids. This theory was used to model wave propagation in fluid saturated, porous rocks where the individual grains are cemented together.

Since then, there has been interest in accurately describing wave propagation in unconsolidated, fluid saturated, porous media, such as water saturated sands. This topic has widespread application in marine seismic surveys and in sonar and underwater acoustics, since portions of the ocean bottom consist of water saturated sand. It is also of interest to soil mechanicists, who use seismic methods to determine the structural properties of sands and soils, both onshore and offshore.

To predict the acoustic properties of these unconsolidated sediments, R. D. Stoll extended Biot's original theory to take into account the losses at the grain-to-grain contacts by proposing that some of the constitutive coefficients in Biot's equations be made complex (Stoll,

1974). Thus, he modeled the solid matrix as a viscoelastic, porous solid, rather than as the porous, elastic solid considered in Biot's original work.

Due to the difficulties encountered when making measurements in saturated sediments, only a limited amount of data exists in publication. Some published data on unconsolidated, fluid saturated, porous media have been produced by R. D. Stoll (Stoll, 1974), David Bell (Bell, 1979), D. J. Shirley (Shirley, 1978; Bedford, 1982), and Jens Hovem and G. D. Ingram (Hovem,1979). More measurements need to be taken, however, both to validate the theory and to determine the physical properties of the sediments.

The present experiment, first proposed by D. J. Shirley, investigates the dependence of the attenuation and phase velocity of compressional waves in a saturated sand on the properties of the interstitial fluid. A mixture of glycerine and water was used as the saturating fluid to permit the controlled variation of the viscosity, density, and bulk modulus of the pore fluid. Since these parameters appear explicitly in the Biot-Stoll equations, this investigation provides a critical test of the theory. Furthermore, the measurements also provide an estimate of some of the constitutive coefficients in the equations.

Similar measurements have been made by Shirley, and later by Elliot (Bedford, 1982). Due to large experimental uncertainties in their results, no definite conclusions could be made. After investigating their procedure, a few simple modifications have been made. New

measurements have been taken and shown to be repeatable within experimental uncertainties.

The most significant development over the earlier work resulted from the redesign of the compressional wave transducers. With this improvement, the existence of spherical spreading was established at the separations at which these measurements were taken and the error caused by the directivity of the transducers was reduced.

Both Shirley and Elliot made shear wave measurements in their investigations. Although it would have been desirable to have measured the attenuation and phase velocity of shear waves, it was decided that we could not substantially improve their earlier results without considerable additional investment in time and effort. Therefore, only compressional wave propagation was considered in this investigation.

This report is organized as follows. A short review of the theory for the compressional wave case is presented in Chapter II. In Chapters III and IV, the experimental procedure is discussed and some of the assumptions are justified. We compare our results to those of other investigators in Chapters IV and V, and in Chapter V our results are compared with the theory.

II. THEORETICAL BACKGROUND

In three articles published in The Journal of the Acoustical Society of America, two in 1956 and the third in 1962, M. A. Biot presented a theory describing the propagation of acoustic waves in a fluid saturated, porous, elastic solid (Biot, 1956a, 1956b, 1962). In this theory, dissipation due to scatter is neglected, requiring that the wavelength be large in relation to the pore size.

Biot predicted three types of body waves in an unbounded, porous medium: two types of compressional waves and one shear wave. All three of these have been observed experimentally. The first type of compressional wave and the shear wave are analogous to the waves predicted by ordinary elasticity. The second type of compressional wave is more dispersive and highly attenuated (Stoll, 1974, 1977).

In Biot's theory, the solid matrix is an elastic frame in which there is no relative motion between the grains. Later, Stoll and Bryan extended this theory to include unconsolidated porous media, such as sands and sediments. Thus, they incorporated into the theory the inelastic nature of the frame, which is caused by the relative motion of the grains.

In the Biot-Stoll theory, losses are attributed to three mechanisms. There are frictional losses at the grain-to-grain contacts. Secondly, the movement of grain particles relative to one another produces fluid motion in their immediate vicinity that does not

contribute to the propagation of the wave. This local fluid motion is at the expense of the propagating wave, and thus it constitutes a loss mechanism.

The third type of loss mechanism, and the one which is thought to dominate in this study, is due to viscous losses in the fluid. This type of absorption becomes important if there is significant motion between the fluid and the skeletal frame. This effect dominates at higher frequencies or in sediments where the permeability is high. For instance, this effect will become more important at lower frequencies for coarse sands than it would for finer sediments and clays, which have a lower permeability.

The main purpose of this report is to compare the experimental measurements of attenuation and phase velocity with the predictions of the theory. What follows is an outline of the derivation of an expression for the wave number from Biot's equations. It will serve only to acquaint those already familiar with the theory with our method of calculating the phase velocity and attenuation, should there arise any discrepancies between our results and those of others. For a more complete discussion, the reader should consult the references by Biot, Stoll, Bedford, and Hovem and Ingram.

In order to present Biot's equations, some of the notation used needs to be introduced. If we let $\underline{u}$ and $\underline{U}$ represent the displacement fields of the solid skeletal frame and the fluid, respectively, and if β is the porosity, then we can write

$$e = \text{div}\,\underline{u} = \nabla \cdot \underline{u}$$

and $$\xi = \beta\,\text{div}\,(\underline{u} - \underline{U}) = \beta\,\nabla \cdot (\underline{u} - \underline{U})$$

Thus, e represents the dilation of an element attached to the frame, and ξ represents "the volume of fluid that has flowed in or out of an element of volume attached to the frame" (Stoll, 1974). The mass density of the fluid-solid mixture is

$$\rho = (1 - \beta)\,\rho_s + \beta\,\rho_f$$

and $$\rho_c = \rho_f/\beta + c/\beta^2$$

where ρ_s and ρ_f represent the density of the solid and fluid, respectively.

The drag and virtual mass coefficients are b and c, respectively. Hovem and Ingram (Hovem, 1979) evaluated b and c as funtions of frequency and showed that

$$b/\beta^2 = \eta\,\text{Real}\,F(\kappa)/B_0$$

$$c/\beta^2 = \eta\,\text{Imaginary}\,F(\kappa)/(\omega B_0)$$

where $$\kappa^2 = a_p^2\,(\omega\rho_f/\eta)\quad,$$

η represents the viscosity, ω is the angular frequency, and B_0 is the permeability. The term a_p, which represents a pore size parameter, is given by

$$a_p = \beta\,d_m/3(1 - \beta)$$

and d_m is the diameter of the spherical grains of the sediment. The

function $F(\kappa)$ can be evaluated in terms of the Kelvin function $T(\kappa)$

$$F(\kappa) = \frac{\kappa\, T(\kappa)/4}{1 - 2\, T(\kappa)/i\kappa} \quad .$$

The Kelvin function is given by

$$T(\kappa) = \frac{ber'(\kappa) + i\, bei'(\kappa)}{ber(\kappa) + i\, bei(\kappa)} \quad .$$

The functions $ber(\kappa)$ and $bei(\kappa)$ are the real and imaginary parts of the zero order Bessel function of the first kind

$$ber(\kappa) + i\, bei(\kappa) = J_0 (\kappa \cdot e^{i3\pi/4}) \quad .$$

The functions $ber'(\kappa)$ and $bei'(\kappa)$ are the derivatives of $ber(\kappa)$ and $bei(\kappa)$, respectively.

Biot's equations contain several constitutive coefficients which can be evaluated in terms of the moduli of the solid matrix and the solid and fluid constituents. The bulk modulus of the drained, solid frame, K_b, and the shear modulus of the drained, solid frame, μ, are made complex in order to account for the inelastic response of the frame. The bulk modulus of the solid and fluid constituents are denoted K_s and K_f, respectively. In terms of these parameters, the constitutive coefficients in Biot's equations can be written (Stoll, 1974)

$$H = \frac{(K_s - K_b)^2}{D - K_b} + K_b + 4\mu/3 \quad ,$$

$$C = \frac{K_s (K_s - K_b)}{D - K_b} \quad ,$$

and $$M = \frac{K_s^2}{D - K_b}$$

where $$D = K_s [1 + \beta (-1 + K_s / K_f)] \quad .$$

With this short introduction to the notation, Biot's equations for compressional waves can be written

$$\frac{\partial^2}{\partial t^2} (\rho e - \rho_f \xi) = \nabla^2 (He - C\xi)$$

$$\frac{\partial^2}{\partial t^2} (\rho_f e - \rho_c \xi) = \nabla^2 (Ce - M\xi) + \frac{b}{\beta^2} \frac{\partial \xi}{\partial t} \quad .$$

To find expressions for the phase velocity and attenuation, harmonic plane wave solutions are assumed for the dilation, e, and the increment of fluid content, ξ, as follows:

$$e = K_1 \exp i(\omega t - kx)$$

$$\xi = K_2 \exp i(\omega t - kx) \qquad (II-1)$$

where K_1 and K_2 are arbitrary constants. Upon substitution into Biot's equations, the wave number, k, can be solved for in terms of the other parameters. In general the wave number is complex. The phase velocity, c_0 and the attenuation, α, can be found from the real and imaginary parts

of the wave number by the following relations:

$$Re(k) = \omega/c_0 \qquad \text{and} \qquad Im(k) = -\alpha \quad .$$

Substituting equations (II-1) into Biot's equations leads to two algebraic equations in e and ξ which can be written

$$(-\omega^2\rho + k^2H)\,e + (\omega^2\rho_f - k^2C)\,\xi = 0$$

$$(-\omega^2\rho_f + k^2C)\,e + (-\omega^2\rho_c - k^2M - ib\omega/\beta^2)\,\xi = 0 \quad .$$

In order that nontrivial solutions to this system of equations exist, it is required that the determinant of the coefficients vanish. Solving this determinant leads to a fourth order algebraic equation in k

$$A_1 k^4 + A_2 k^2 + A_3 = 0$$

where $A_1 = C^2 - MH$,

$$A_2 = \omega^2(\rho M + \rho_c H - 2\rho_f C) - i\omega Hb/\beta^2 \quad , \qquad \text{(II-2)}$$

and $$A_3 = (i\rho\omega^3)b/\beta^2 + \omega^4(\rho_f^2 - \rho\rho_c) \quad .$$

The roots to this equation are given by the quadratic formula

$$k^2 = [-A_2 \pm \sqrt{(A_2^2 - 4A_1A_3)}\,] / 2A_1 \quad . \qquad \text{(II-3)}$$

This represents four roots, two positive and two negative.

The two positive roots correspond to two different compressional waves. The value of k calculated from the negative value of the discriminant, $-\sqrt{(A_2^2 - 4A_1A_3)}$, corresponds to the compressional wave of the second type, or the compressional slow wave. Since the present experiments are designed to measure the velocity and

attenuation of the compressional wave of the first type, the wave number was calculated with the positive discriminant.

The FORTRAN program shown in Appendix A was used in order to solve the quadratic formula (II-3) with coefficients (II-2) as a function of viscosity. The program displays the results in graphical form. In order to solve for the wave number, and thus the phase velocity and attenuation, the physical parameters of the saturated sediment need to be determined. This process is discussed more fully in Chapter V. In the next two chapters the procedure used to measure these quantities is discussed in detail.

III. LABORATORY EQUIPMENT

A. General Procedure

The objective of this experiment is to determine the phase velocity and attenuation of harmonic, compressional waves in a fluid saturated sediment as a function of the properties of the pore fluid. These results will be compared with those predicted by the Biot-Stoll theory. Since the fluid viscosity, bulk modulus, and density appear in the expression for the wave number, these measurements are expected to be a critical test of the theory.

Similar measurements of the acoustic properties of sediments have been performed by Bell (Bell, 1979), Shirley, and Elliot (Bedford,1982). The main focus of the work described in this chapter and the next has been to improve the techniques developed by these investigators for measuring the attenuation and phase velocity of compressional waves and to locate the causes of experimental error. The most significant improvement over the earlier work has resulted from the redesign of the compressional wave transducers. With this improvement, spherical spreading was established at the separations at which these measurements were taken and the error caused by the directivity of the transducers was reduced.

The two transducers are essentially identical. One serves as a transmitter and the other as a receiver. The transmitter converts an electrical signal, which is generated in an oscillator, into an acoustic signal, which propagates through the sediment. The receiver detects this

acoustic signal and reconverts it into an electrical signal which is displayed on an oscilloscope.

The central idea in our measurement procedure is to compare the time delay and amplitude of the output voltage signal at one transducer separation with the same measurements at other separations. From the time delay measurements at different separations, the phase velocity is determined. Similarly, by comparing the different amplitude measurements, the attenuation can be calculated. It is assumed that the coupling between the transducer and sediment is the same at each separation. Thus we assume that the decay in amplitude is due only to the increase in transducer separation.

Initially, the transducers are placed 20.0 cm apart. The time delay from the beginning of the triggered pulse to the fourth positive peak of the received signal is then recorded along with the peak-to-peak amplitude of the fourth cycle of the received signal. The fourth cycle is used so that the measurements are made as close to the steady state part of the signal as possible. The signal is then monitored for at least four hours to ensure that there are no variations in the signal amplitude due to changes in the coupling between the sediment and the transducers or due to any settling of the sediment. Four to six readings are taken over this period, and the slight variations about the stabilized value are averaged. The receiver is then moved 2.0 cm closer to the transmitter and the amplitude and time delay measurements are repeated. The entire procedure is repeated at 2.0 cm intervals until the separation between the transducers has been reduced to 6.0 cm. Using this set of

measurements, the phase velocity and attenuation are determined by finding the least squares fit to the data.

The fluid properties are then altered by adding glycerine to the mixture. The entire set of measurements is repeated and the phase velocity and attenuation are determined for a new value of viscosity. This procedure is repeated several times, each time with a new value of viscosity. In this way, plots of phase velocity and attenuation versus viscosity can be made and then compared with predictions of the theory.

B. Instrumentation

A schematic of the laboratory equipment is shown in Fig. 1. A continuous tone of 105.0 kHz and 10.0 v peak-to-peak amplitude is generated in the oscillator. The output is sent to a frequency counter and a tone burst generator. The tone burst generator passes a four cycle pulse of 105.0 kHz to a transmitting transducer and an oscilloscope. The signal is then cut off for several milliseconds so that the reflections of the signal off of the sides of the container and the sediment-water interface will die down before a new four cycle pulse is sent to the transmitter. If the reflections are not suppressed, they will interfere with the signal that follows the direct path between the transducers and produce an error in the signal amplitude and time delay measurements.

The pulse is also displayed on an oscilloscope. The tone burst generator has a synchronized output, which is connected to the external

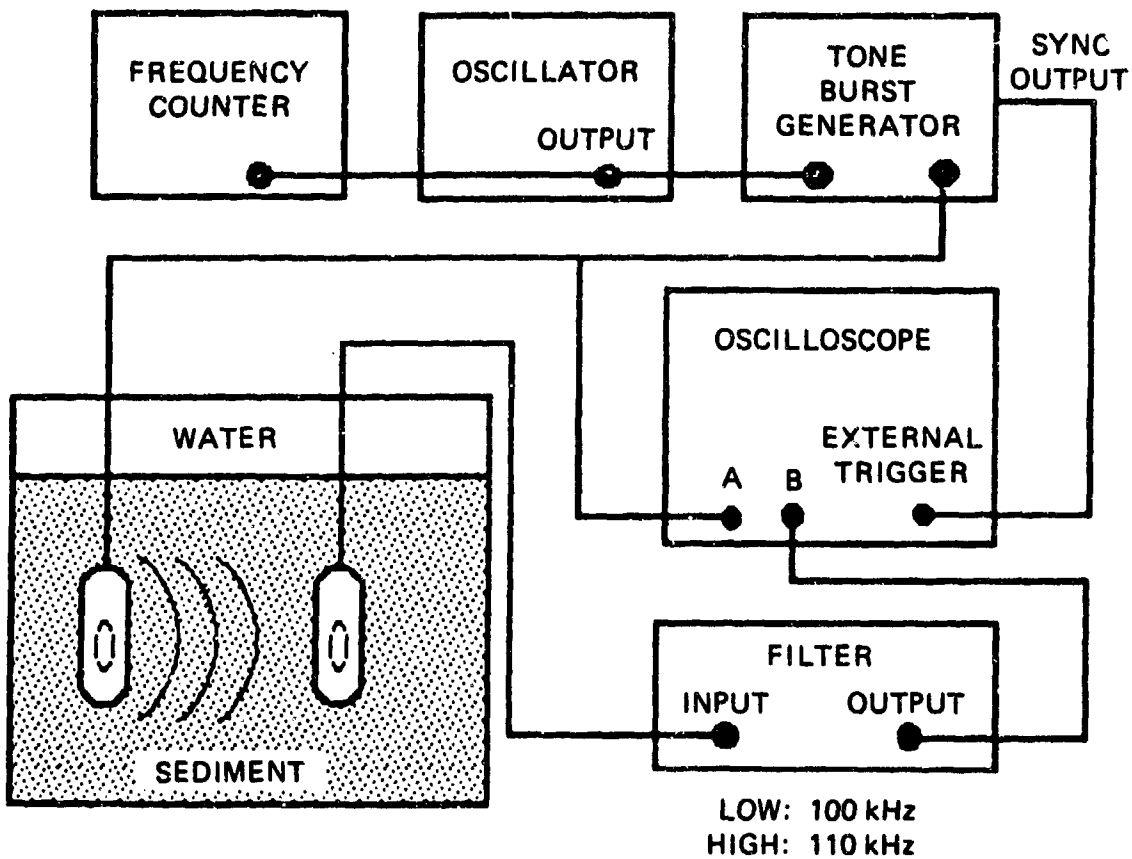

FIGURE 1
SCHEMATIC OF EXPERIMENTAL EQUIPMENT

ARL:UT
AS-85-54
RDC - GA
1 - 23 - 85

trigger input of the oscilloscope. This causes the oscilloscope trace to trigger at the beginning of the four cycle pulse.

The acoustic pulse generated in the sediment is then detected by the receiving transducer. The transducer translates the acoustic signal into a voltage which is sent through a bandpass filter and then displayed on the oscilloscope. The low and high cutoff frequencies of the bandpass filter are 100 kHz and 110 kHz, respectively. The filter is used to remove the extraneous frequencies, introduced because the transmitted pulse is the product of a pure tone and the difference of two step functions, from the received signal.

C. Transducers

1. Construction. The two transducers are nearly identical and can be used as either transmitters or receivers. The transducers were built from a piezoelectric element mounted in a stainless steel plate. A rod was welded onto the plate so that the plate and transducer element could be inserted into the sediment-water mixture. A sketch of a transducer mount is shown in Fig. 2.

The two elements are made of the material Channelite 5500 and manufactured by Channel industries, Inc. Their thickness and diameter are 3/16 in. and 3/4 in., respectively. They each have two resonances. In the thickness mode, #1 and #2 resonate at 446.4 kHz and 445.2 kHz, respectively. In the radial mode, #1 and #2 resonate at 105.5 kHz and 105.1 kHz, respectively. In this experiment, the transducers are used in the radial mode, at 105.0 kHz.

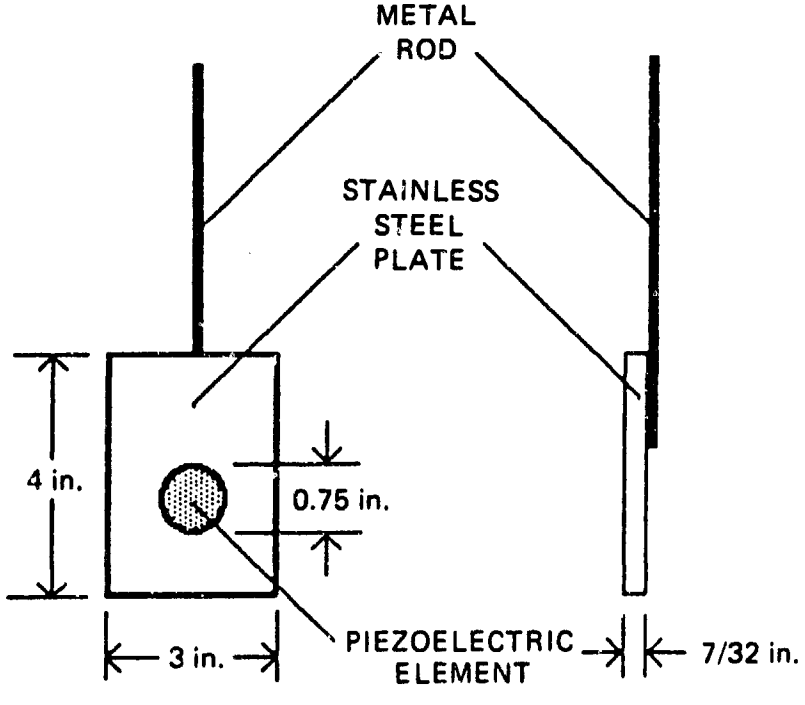

FIGURE 2
DIMENSIONS OF TRANSDUCERS

To build the transducers, a 7/8 in. hole was drilled through the steel plate. The element was placed in the hole with corprene placed between it and the steel plate, around the circumference of the element, and behind it on the backside of the transducer. A wire was soldered on each face of the element, and the two wires were placed in a shielded, waterproofed sheath.

The corprene is of much lower acoustical impedance than either the piezoelectric element or the sediment-water mixture. It was thus used on the backside of the element to act as a pressure release material so that most of the radiation would be from the front side of the transducer. This directs most of the energy toward the receiver, producing a higher signal to noise ratio.

The area of the plate was made sufficiently large and thick, and the shape of the element was chosen to be circular, so that radiation from the transducer could be treated as radiation from a piston in a rigid baffle. In this way the geometrical spreading and the directivity of the transducer could be calculated and verified by measurement.

2. Geometrical Spreading. Since the geometrical spreading in the nearfield is very complicated and varies with distance from the source, the transducers were designed for use in the farfield. The Rayleigh distance is roughly the distance away from the source at which the farfield begins. At separations larger than the Rayleigh distance, the amplitude of the signal decays as 1/r, due to the geometrical spreading of the signal.

The Rayleigh distance for a circular piston in an infinite, rigid baffle is given by (Blackstock)

$$R = {}^1/_2\, ka^2$$

where a is the radius of the piston, $k=\omega/c_0$ is the wave number, and ω is the angular frequency. Note that R is inversely proportional to the phase velocity c_0. For these transducers, and a frequency of 105.0 kHz, this formula gives a Rayleigh distance of 2.0 cm in water. Thus, spherical spreading is expected at separations of about 4.0 cm or greater.

For a lossless medium in which there is 1/r spreading, the signal amplitude satisfies the following relation:

$$\frac{E}{E_r} = \frac{K\lambda}{r}$$

where E is the signal amplitude, E_r is a reference amplitude, λ is the wavelength, and K is a calibration constant. Taking the logarithm of both sides gives

$$\log \frac{E}{E_r} = -\log \frac{r}{\lambda} + \log K .$$

Thus, if the signal amplitude is measured as a function of separation for separations greater than the Rayleigh distance, the points will fall on a straight line with a slope of -1 when plotted on log-log graph paper. Thus, to experimentally verify that there is spherical spreading in water at separations greater than 4.0 cm, the amplitude of

the acoustic signal was measured as the separation was varied from 4.0 cm to 20.0 cm, in 2.0 cm increments. A least squares fit through the points on a log-log plot of range versus amplitude revealed a slope of m=-.9914 of the equation.

$$\log \frac{E}{E_r} = m \times \log \frac{r}{\lambda} + \log K \quad .$$

If the point corresponding to r = 4.0 cm is omitted, the slope is m=-1.0061 as shown in Fig. 3. At these distances, it can be assumed that there is no absorption in water and the total losses can be attributed to geometrical spreading. Therefore, this test shows that there is spherical spreading at separations greater than 4.0 cm.

Since the phase velocity is greater in the sediment-water mixture than in water, the Rayleigh distance is even smaller in the mixture. These considerations establish that spherical spreading in the sediment is a good assumption at separations greater than 4.0 cm.

3. Directivity. Since the transducers are directional and the receiving transducer is moved to a new separation after each set of readings, great care has to be taken so that the transducers remain on each others axes, where the signal amplitude is maximum. The axis is the imaginary line running through the center of the circular element and perpendicular to its face. The alignment problem is lessened if the radiation pattern of the transducer is sufficiently wide that slight

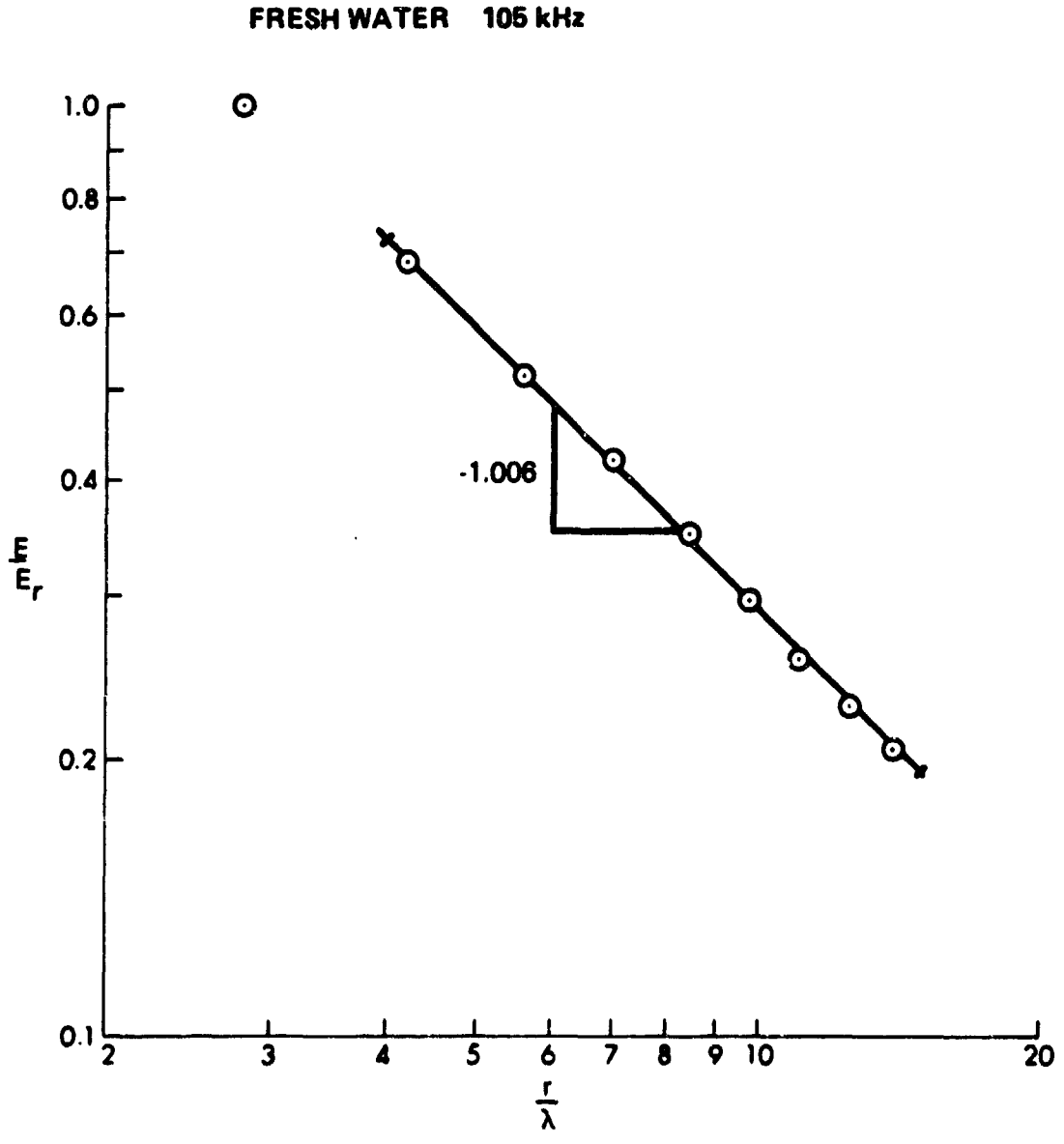

$$\log \frac{E}{E_r} = -\log \frac{r}{\lambda} + \log K$$

$$E = \frac{\lambda K E_r}{r} = \frac{K'}{r}$$

FIGURE 3
SPHERICAL SPREADING IN FRESH WATER

ARL:UT
AS-84-1035
DRC-GA
11-19-84

errors in realigning the receiver exactly on the axis of the transmitter will cause only slight error in measuring the on-axis signal amplitude.

By treating the transducer as a circular piston in an infinite, rigid baffle, the half-power angle can be calculated. If p(0,r,t) is the on-axis pressure, then the half-power angle is the angle at which the pressure is given by (Blackstock)

$$p(\theta_{HP},r,t) = p(0,r,t)/\sqrt{2} \quad .$$

For a circular piston, the half-power angle is (Blackstock)

$$\sin \theta_{HP} = 1.616/ka \quad .$$

In fresh water, at a frequency of 105.0 kHz, the calculated half-power angle for these transducers is 22.6°.

Figures 4 and 5 show the measured directivity of the two transducers in fresh water. Again, it is seen that the model of the transducer as a circular piston in a rigid baffle works well. The directivity patterns for both transducers show that the half-power angle, the angle at which the pressure is 3.0 dB below the on-axis pressure, is about 20°.

Since transducer #1 is used as the receiver in this experiment, and is moved after each reading, it is desired that the response of this transducer especially be constant for small angles off axis. This is so that failure to exactly realign the transducers will still give a reliable measurement of the on-axis value of the signal amplitude. Fig. 4 shows that the sound pressure level, L_p, for transducer #1 varies less than

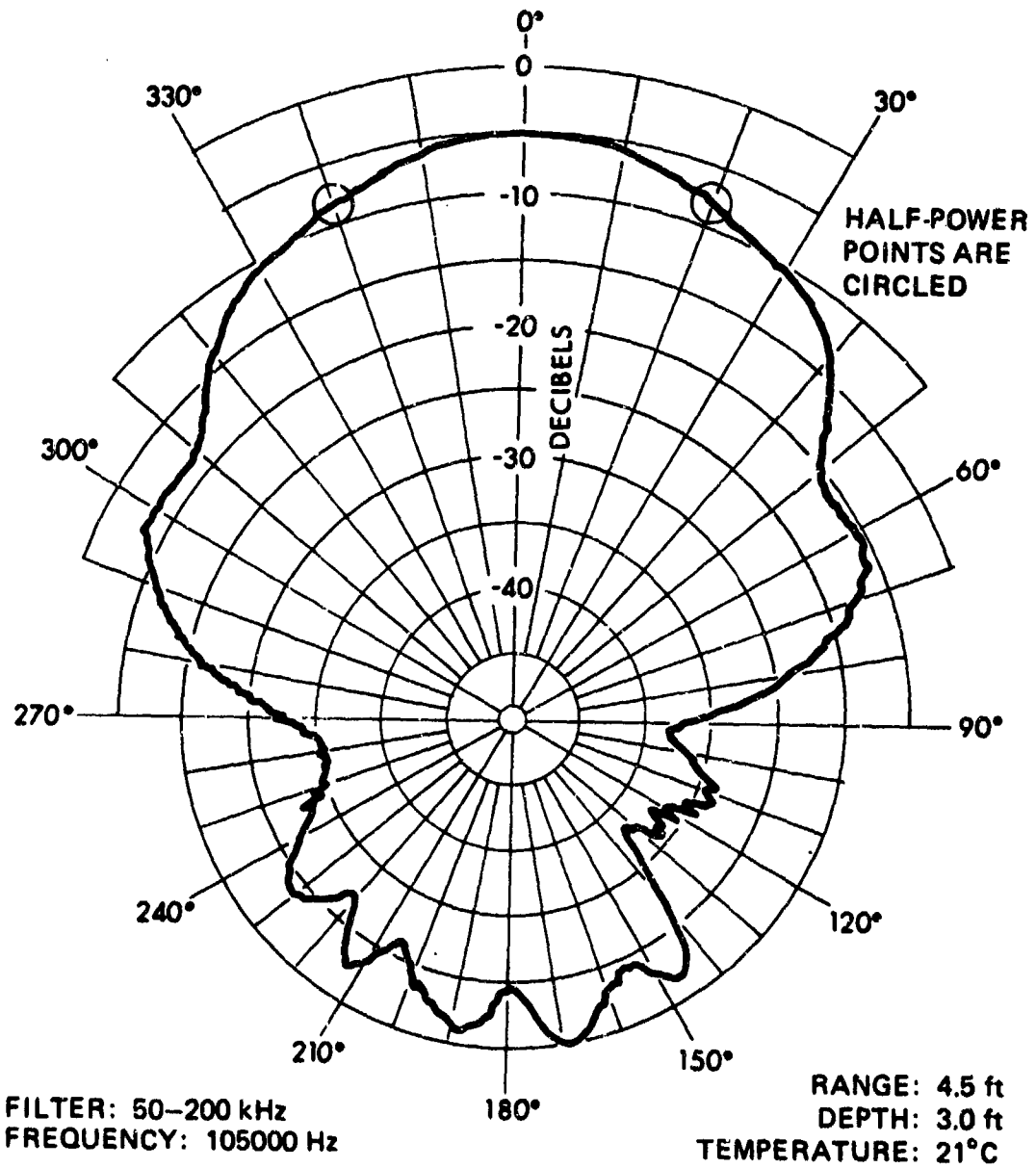

FIGURE 4
DIRECTIVITY PATTERN IN HORIZONTAL PLANE
FOR TRANSDUCER No. 1 IN FRESH WATER

ARL:UT
AS-85-58
RDC - GA
1 - 23 - 85

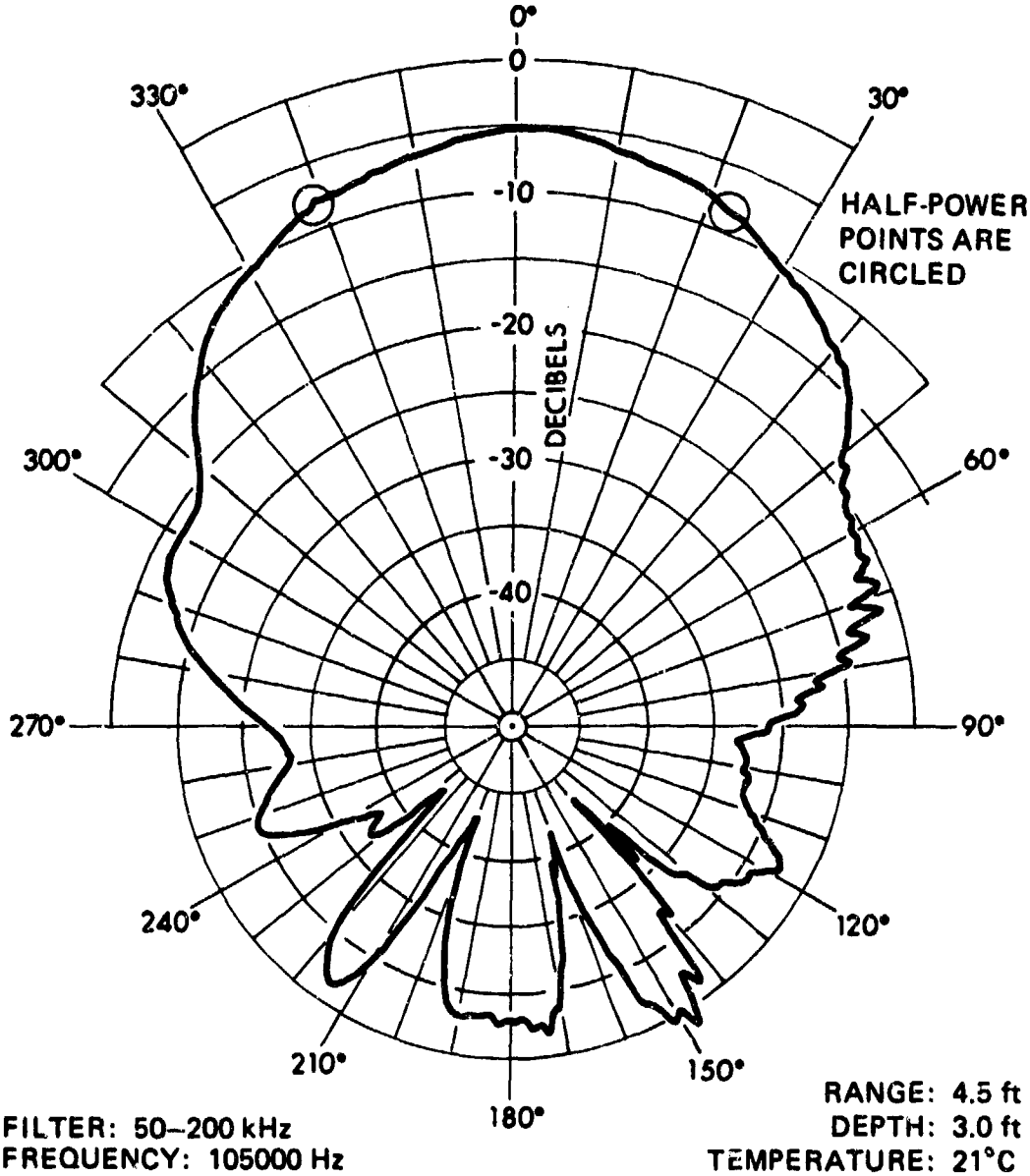

FIGURE 5
DIRECTIVITY PATTERN IN HORIZONTAL PLANE
FOR TRANSDUCER No. 2 IN FRESH WATER

ARL:UT
AS-85-57
RDC - GA
1 - 23 - 85

0.5 dB for 7.0° on either side of the axis. A 0.5 dB difference in L_p implies that the actual pressure varies less than 6.0% from the on-axis value. Actually, the L_p for transducer #1 is essentially constant for angles up to 3.0° off axis.

For media such as saturated sediments, in which the sound speed is higher than that of water, the half-power angle would be even greater. A typical compressional wave speed for a sediment-water mixture is 1800 m/s (Bell, 1979). At the same frequency that is being considered, 105.0 kHz, this leads to a half-power angle of 28°. Thus one is led to believe that for small angles off axis, the signal amplitude would vary even less in the mixture than it would in water. In the measurements taken in this investigation, it was estimated that the receiver was positioned in the sediment with no more than 4° variation in the angle off axis. Thus, there is confidence that the on-axis signal amplitudes were measured accurately.

D. Sediment Preparation

The experimental sediment is made up of MS-MH size glass beads manufactured by the Ferro Corporation of Jackson, Mississippi. The grain size distribution is shown in Fig. 6 (Bell, 1979).

The sediment-water mixture was prepared in a five gallon, plastic bucket in the following manner. The bucket is approximately 35 cm high and 29 cm in diameter. The liquid in the sediment-water mixture is circulated by a Masterflex tubing pump. Before the mixture was put in the bucket, the outflow tube was attached to the bottom

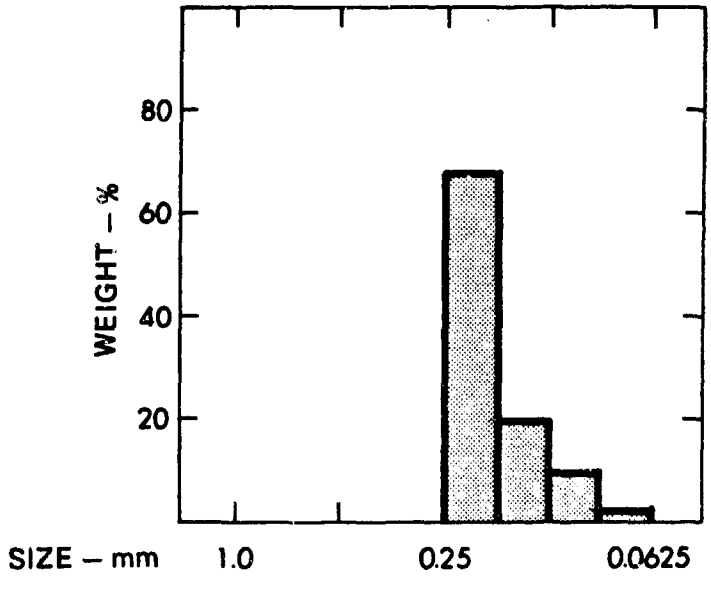

FIGURE 6
GRAIN SIZE DISTRIBUTION FOR MS-MH SIZE BEADS

of the bucket with duct tape. The bucket was then partially filled with de-ionized water and the input hose was put in the water. The pump was turned on so that all of the air was driven from the tube. To retard the growth of micro-organisms, 20 ml of BIO-CLEAN III algaecide was added to the water.

The glass shot was then poured slowly into the water until the sediment-water mixture was 24 cm deep. Pouring was halted at intervals and the mixture kneaded to remove air trapped in the beads. A layer of water, approximately 6 cm thick, was left on top of the sediment mixture and the input hose to the pump was suspended in the layer, as shown in Fig. 7.

The bucket was then placed inside a vacuum tank on top of a vibrator to remove any air remaining in the mixture. The tank was evacuated and the mixture was vibrated in excess of 6 hours. The mixture was left in the vacuum overnight, but the vibrator was turned off. After the sediment was removed from the vacuum, the transducers were inserted into the mixture so that the center of the elements were 12 cm below the sediment-water interface.

To alter the fluid properties, glycerine was poured into the liquid on top of the mixture and the pump turned on until the liquid in the bucket was well mixed. Approximately 10 ml of algaecide was added while the liquid was being circulated to further retard the growth of micro-organisms. The specific gravity of the liquid was measured several times while the liquid was being circulated. The liquid was considered well mixed after the values of specific gravity had stabilized.

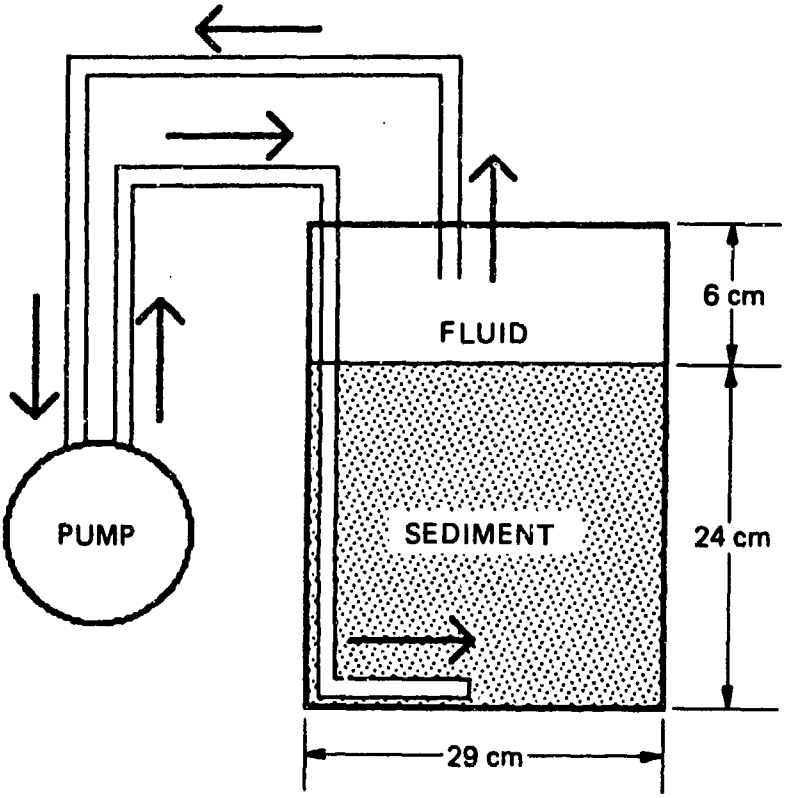

FIGURE 7
CIRCULATING THE PORE FLUID

ARL:UT
AS-85-59
RDC - GA
1 - 23 - 85

This usually occurred after about 3 hours. The specific gravity was measured using a hydrometer and the value of viscosity was determined from a table containing values of viscosity for varying concentrations of glycerine-water solutions (Sheely, 1932).

IV. EXPERIMENTAL PROCEDURE

A. Phase Velocity

The oscilloscope trace is triggered at the beginning of the transmitted four cycle pulse. The delay time to the fourth positive peak on the received signal is measured with a digital readout on the oscilloscope. This is first done at a transducer separation of approximately 20 cm, and then at every 2.0 cm increment down to a separation of 6 cm. If these delay times are then plotted on a time versus distance graph, with time as the horizontal axis, the points should fall on a straight line parallel to the characteristic of the wavelet. The slope of this line is the phase velocity.

Therefore, to find the phase velocity a least squares routine is used to fit the best straight line through these points. Since the line is parallel to a characteristic, the equation of the line is of the form

$$r = c_0 t + B$$

where c_0 is the phase velocity, B is the intercept of the r-axis, and r and t represent the separation and time delay, respectively. If the time were measured from the fourth positive peak on the transmitted pulse to the same peak on the received pulse, B would ideally be zero (for a nondispersive medium) and the least squares line would be the same as the characteristic. But since time is measured from the beginning of the triggered pulse and there are additional time delays associated with the circuitry and transducers, B turns out to be negative.

This method was tested using two different size beads with fresh water as the pore fluid: the MS-MH size which was used in the experiment, and the MS-L size which are smaller size beads. The results of these preliminary tests are shown in Figs. 8 and 9. The linear correlation coefficient displayed in the figures is a number between zero and one that gives an indication of how well the data points fit a straight line. A coefficient of one represents perfect linear correlation and a coefficient of zero represents no correlation. The coefficients shown in the figures indicate a very good correlation between the data and the straight lines. The good correlation suggests that the disturbances in the sediment, caused by moving the transducer to each separation, have a negligible effect on the measurement

In order to check the validity of our procedure, we measured the phase velocity in water at room temperature, approximately 25°C, six times. Each of these results were between 1492 m/s and 1508 m/s. The average of these measurements was 1501 m/s. By linear interpolation of tabulated values of sound speed as a function of temperature (AIP Handbook, 1963), the speed of sound at 25°C in fresh water is 1496 m/s. The average then has an error of only 0.33%, while the extreme values have errors of -0.3% and 0.8%.

In another check, we compared our results to results obtained by Bell (Bell, 1979), Shirley (Bedford, Appendix A, 1982), and Hovem and Ingram (Hovem, 1979). We measured the phase velocity three separate times in MS-MH beads with fresh water as the pore fluid. The three results are shown in Table I, along with the other results mentioned.

BEAD TYPE: MS-MH
FREQUENCY: 105 kHz VISCOSITY: 0.893 cP

TIME -- μs	SEPARATION -- cm
65.88	5.65
77.63	7.65
88.98	9.65
100.12	11.65
112.07	13.65
121.38	15.65
133.23	17.65
142.31	19.65

VELOCITY: 1820 m/s
STANDARD DEVIATION OF VELOCITY: 24 m/s
LINEAR CORRELATION COEFFICIENT: 0.9995

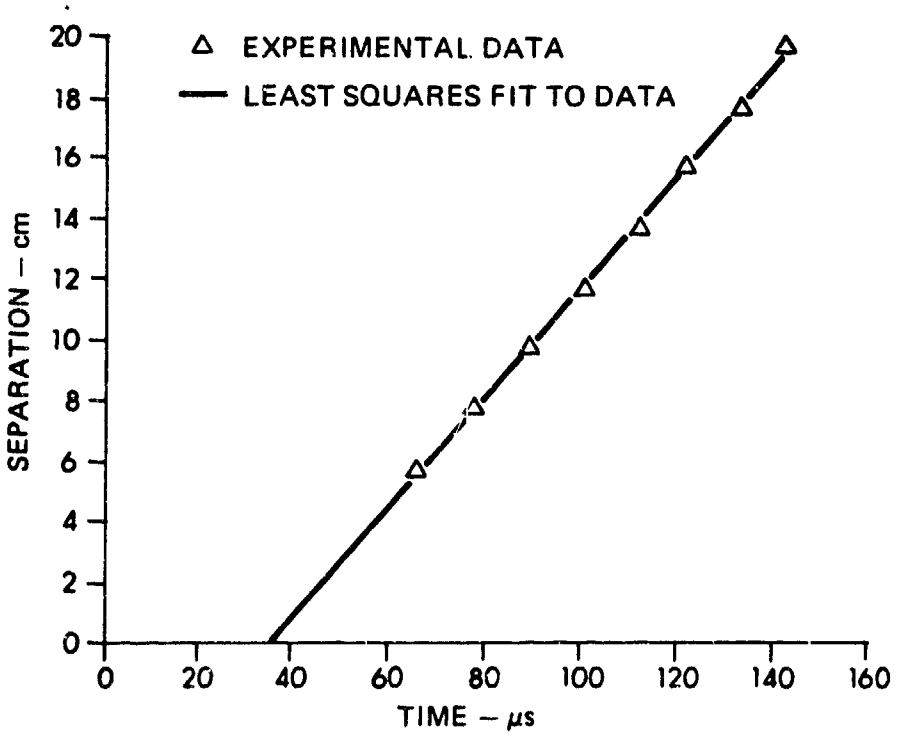

FIGURE 8
PHASE VELOCITY IN MS-MH BEADS

BEAD TYPE: MS-L
FREQUENCY: 105.0 kHz VISCOSITY: 0.893 cP

TIME – μs	SEPARATION – cm
63.62	5.65
73.39	7.65
83.49	9.65
95.51	11.65
107.15	13.65
118.60	15.65
131.73	17.65
138.98	19.65

VELOCITY: 1791 m/s
STANDARD DEVIATION OF VELOCITY: 34 m/s
LINEAR CORRELATION COEFFICIENT: 0.9989

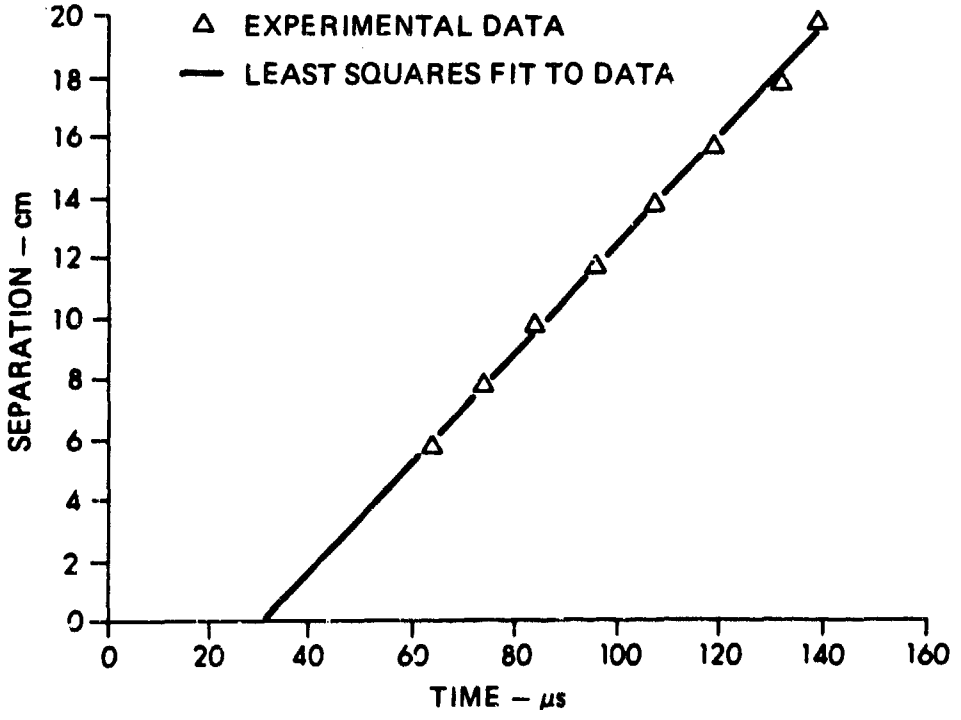

FIGURE 9
PHASE VELOCITY IN MS-L BEADS

Comparison with these other results indicates that our results are valid. But the comparison also suggests that the velocity is strongly dependent on the depth of the transducers in the sediment.

The comparison in the MS-L size beads is not nearly so good. Our first trial measurement in sediments was made in the MS-L size beads. Since the standard deviation accompanying this measurement is so large, 34 m/s, and since in all subsequent measurements the standard deviation was substantially reduced, the discrepancy is attributed to experimental error and carelessness in precisely determining the separation. As the experiment progressed, the technique improved and the error decreased.

Table I: Comparison of Velocity Results in MS-MH and MS-L Size Beads.

	Frequency - kHz	Depth - cm	Velocity - m/s	
			MS-MH	MS-L
Bell	120.	9	1809	1854
Shirley	114.	10	1808	
Hovem & Ingram	100.	20	1922	
Present Study	105.	12	1820	1791
	105.	12	1840	
	105.	12	1866	

Obviously, the sound speed measurements in sediments are not nearly as repeatable as the measurements made in water. One reason for this is the uncertainty in the separation measurement. In the sediment, this uncertainty is estimated to be 0.1 cm. At a separation of 20 cm this represents a relative uncertainty of 0.5 %, while at 6 cm the uncertainty is 1.7%. The uncertainty in the time delay measurement is negligible compared to this. Relative uncertainties of 0.5% and 1.7% in the separation represent absolute uncertainties of 10 m/s and 30 m/s in the velocity, respectively.

The standard deviations shown in Figs. 8 and 9 were derived from the least squares method. In this calculation of the uncertainty it was assumed that the uncertainties in the time delay measurements, which were measured along the horizontal axis, were negligible. It was also assumed that the absolute uncertainties of each of the separation measurements, which were represented on the vertical axis, were equal. Since both of these assumptions are appropriate and the standard deviations calculated from the least squares method are consistent with uncertainties in the separation measurements, these standard deviations are a realistic measure of the uncertainty in the velocity.

All of the velocity measurements made in the sediments are listed in Table VII of Chapter IV and in Appendix B together with the raw data. It can be seen that the standard deviations of the velocities were less than 15 m/s after the first few trial measurements. This indicates that as the experiment progressed, the technique was improved and the uncertainty decreased.

B. Attenuation

1. Measurement Technique. In the sediment the losses are due to both geometrical spreading and absorption of the medium. Therefore, to calculate the attenuation by the medium the geometrical spreading must be taken into account. As discussed in Section III.C.2., the transducers were designed so that the Rayleigh distance would be relatively small compared to the sediment sample. At distances greater than the Rayleigh distance, the signal amplitude decays as 1/r due to spherical spreading, where r is the separation between the transducers. This distance was calculated for both water and the sediment. The calculation for water was then verified by acoustic measurements. These measurements support the calculated assumption that the geometrical spreading in the sediment is indeed spherical at the distances at which the attenuation measurements are taken. Using spherical spreading, the losses due to absorption in the sediment can be determined. A detailed discussion of this procedure follows.

The measurements establishing the 1/r decay of the signal amplitude due to spherical spreading have been discussed in Section III.C.2. We determine the absorption due to the medium by measuring the amplitude of the signal and assuming that the amplitude varies as

$$E = (K/r)\, e^{-\alpha r} \qquad \text{(IV-1)}$$

in an absorbing medium. Here, K is a calibration constant with units of volts×length and α is the attenuation in nepers per unit length. The 1/r factor in Eq. (IV-1) takes into account the spherical spreading and the

$e^{-\alpha r}$ term takes into account the absorption of the medium. It is also assumed that the coupling between the sediment and the transducer is the same at each separation. Thus, the decay in amplitude of the signal is attributed only to the increase in separation.

The attenuation is determined by comparing the amplitudes measured at various separations. To do this, one of the amplitude measurements and the separation at which it is measured are designated as reference values, E_r and r_r, respectively. In this experiment, r_r is the smallest separation at which measurements are taken and $E_r = E$ at $r = r_r$. Therefore the following relation holds:

$$E_r = (K/r_r)\, e^{-\alpha r_r} \quad .$$

From this and Eq. (IV.1) it follows that :

$$K = E\, r\, e^{\alpha r} = E_r\, r_r\, e^{\alpha r_r}$$

$$e^{\alpha(r-r_r)} = E_r\, r_r/(E\, r)$$

$$\alpha(r-r_r) = \ln [E_r\, r_r/(E\, r)] \quad . \quad \text{(IV-2)}$$

Therefore, if $\ln[E_r r_r/(E\, r)]$ is plotted versus $(r-r_r)$, the points should fall on a straight line and the slope of this line is the attenuation. To find the slope of this line, and thereby the attenuation, the method of least squares can again be employed.

This technique was tested using two different size beads with fresh water as the pore fluid: the MS-MH size which was used in the experiment, and the MS-L size which are smaller size beads. The results of these preliminary tests are shown in Figs. 10 and 11. As in the case of the phase velocity, a linear correlation coefficient near one indicates a very close correlation between the data and the straight line.

The standard deviation can be calculated for this method, assuming that the uncertainties in each of the data points are equal and that there are no errors in the values along the horizontal axis. Because of these assumptions, the standard deviation calculated from the least squares method is too low. But the attenuation can be calculated by other means, and from these calculations a realistic estimate of the error can be made. These methods and the uncertainties associated with them will be discussed in the remainder of this section.

A physical interpretation of the sources of error can be acquired by calculating the attenuation, α, directly using Eq. (IV-2) with the data at any two separations. If the data for MS-MH beads corresponding to separations of 5.65 cm and 19.65 cm, shown in Fig. 11, are used, the attenuation calculated from Eq. (IV-2) is 2.28 Np/m. We can calculate a Pythagorean estimate of the uncertainty in the attenuation from this calculation by using the relation (Bevington, Eq. 4-9, 1969)

$$\sigma_i^2 (r-r_r)^2 = \sigma_r^2(\alpha^2+2\alpha/r+1/r^2)_{ref} + \sigma_r^2(\alpha^2+2\alpha/r+1/r^2) + (\sigma E/E)^2_{ref} + (\sigma E/E)^2 \qquad \text{(IV-3)}$$

where σ_E and σ_r denote the uncertainties, or standard deviations, in the

BEAD TYPE: MS-L
FREQUENCY: 105.0 kHz VISCOSITY: 0.893 cP

AMPLITUDE – V	SEPARATION – cm
0.2800	5.65
0.1970	7.65
0.1430	9.65
0.1060	11.65
0.0820	13.65
0.0652	15.65
0.0516	17.65
0.0430	19.65

ATTENUATION: 4.71 Np/m
STANDARD DEVIATION OF ATTENUATION: 0.14 Np/m
LINEAR CORRELATION COEFFICIENT: 0.9974

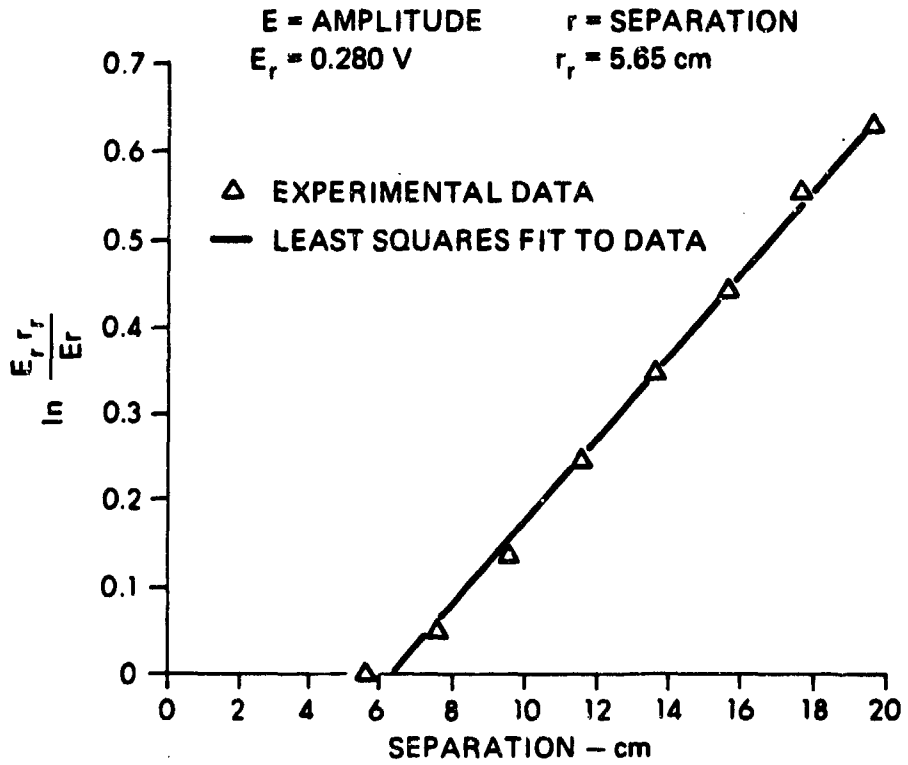

FIGURE 10
ATTENUATION IN MS-L BEADS

BEAD TYPE: MS-MH
FREQUENCY: 105.0 kHz VISCOSITY: 0.893 cP

AMPLITUDE – V	SEPARATION – cm
0.3720	5.65
0.2690	7.65
0.2004	9.65
0.1570	11.65
0.1300	13.65
0.1074	15.65
0.0892	17.65
0.0777	19.65

ATTENUATION: 2.40 Np/m
STANDARD DEVIATION OF ATTENUATION: 0.09 Np/m
LINEAR CORRELATION COEFFICIENT: 0.9962

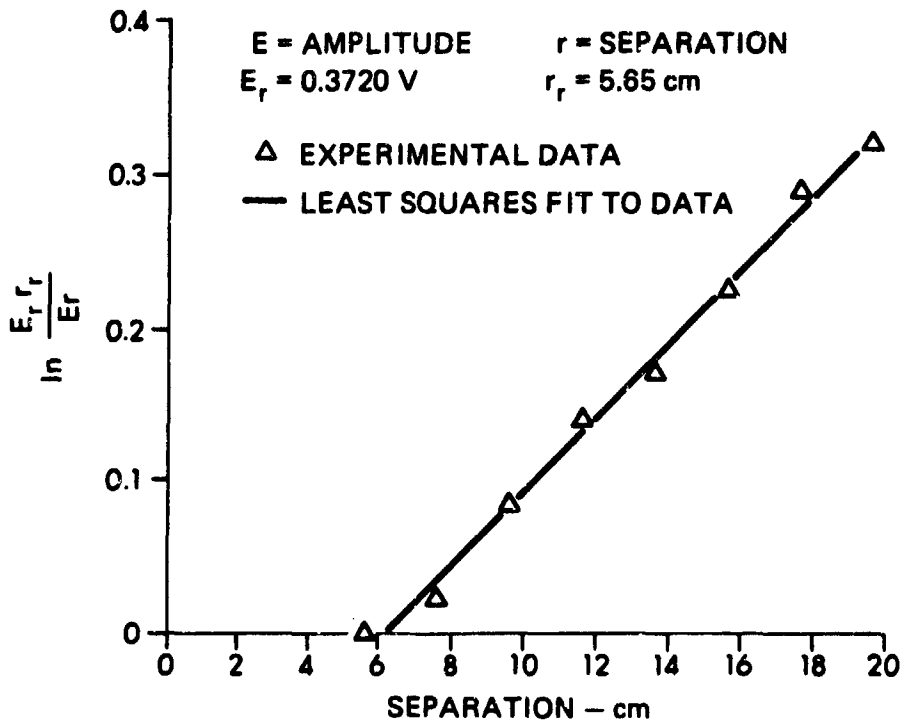

FIGURE 11
ATTENUATION IN MS-MH BEADS

ARL:UT
AS-85-63
RDC - GA
1 - 23 - 85

amplitude and separation, respectively, and the quantities marked "ref" signify that the separations and amplitudes correspond to the separation of 5.65 cm. To perform this calculation, the uncertainties in the separation and the amplitude, σ_r and σ_E, must first be determined. The uncertainty in the separation is estimated to be 0.1 cm.

The uncertainty in the amplitude has two sources. The first one is instrumental, because the oscilloscope can be read accurately to 1/4 of a gradation. The scale is changed at different separations, since the amplitude grows with decreasing r, so this type of uncertainty increases with decreasing separation.

The second source of uncertainty in E is due to the uncertainty in r. Since the amplitude is a function of r, as was assumed in Eq. (IV-1), any uncertainty in r produces an uncertainty in E. This type of error can be estimated from the relation (Bevington, Eq. 4-9, 1969)

$$\sigma_E = \sigma_r \, {}^{\partial E}/_{\partial r} = \sigma_r \, E \, (\alpha r + {}^{1}/_{r}) \quad .$$

By calculating this uncertainty, and comparing the results with the instrumental uncertainty in E, it can be seen that over 80% of the uncertainty in E is due to the uncertainty in r. Using Eq. (IV-3), and the values in the rows in Table II corresponding to r=19.65 cm and r=5.65 cm, the uncertainty in the direct calculation is found to be 0.522 Np/m. Note from Eq. (3) that the uncertainty, σ_i, is inversely proportional to the difference between the two separations being compared. Thus, one way to improve the measurements would be to increase the distances over which the measurements are taken.

Using each pair of data shown in Fig. 11, the attenuation can be calculated seven times in this way, and the values designated as α_i. These seven values of attenuation can then be weighted with their corresponding uncertainties, σ_i, and averaged as shown in Table II (Bevington, p. 73, 1969). The resulting average is a better estimate of the attenuation than any of the individual attenuations, and the standard deviation calculated from this method is a better estimate of the uncertainty. Although this value of α differs by 5% from the least squares value, this standard deviation is a more realistic estimate of the uncertainty.

Table II: Analysis of Errors in Attenuation.

r - cm	E - volts	$\sigma_E/_E$	$\sigma_r\sqrt{(\alpha^2+2\alpha/_r+1/_{r^2})}$	σ_i - Np/m	α_i -Np/m
5.65	0.372	0.0380	0.000404		
7.65	0.269	0.0407	0.000239	3.06	1.057
9.65	0.2004	0.0460	0.000163	1.606	2.082
11.65	0.157	0.0429	0.000121	1.029	2.317
13.65	0.130	0.0478	0.000095	0.813	2.116
15.65	0.1074	0.0533	0.000077	0.690	2.235
17.65	0.0892	0.0592	0.000065	0.613	2.408
19.65	0.0777	0.0587	0.000056	0.522	2.283

$$\sigma_\alpha^2 = \frac{1}{\sum (1/\sigma_i)^2} \qquad \text{so that} \quad \sigma_\alpha = 0.296 \text{ Np/m}$$

$$\alpha = \sigma_\alpha^2 \sum (\alpha_i/\sigma_i^2) = 2.266 \text{ Np/m}$$

In calculating the attenuation using this method, the error in the reference separation and amplitude is repeated in each of the seven calculations. Thus, if reference measurements are particularly bad, the error in them will be compounded in the final result. To avoid this type of error, the attenuation can be calculated with any two pairs of data, E and r. The values corresponding to r = 5.65 cm do not necessarily need to be the reference separation and amplitude. Since there are eight pairs of data, there are 28 possible ways to calculate α using Eq. (IV-2). The unweighted mean of these 28 attenuations and the standard deviation of this mean can be easily calculated. For the MS-MH beads of Fig. 11, this mean is α = 2.38 Np/m and the standard deviation is σ_α = 0.47 Np/m. This value of the attenuation differs only by 0.6% from the least squares value. But this standard deviation is larger than the one calculated from the weighted averages. This may signify that the estimate of the uncertainty in r used in that calculation, σ_r = 0.1 cm, was too low. In later calculations, however, there is better agreement between these two calculations of the standard deviation. This suggests that the separation was determined more precisely as the experiment progressed. Another reason for the discrepancy is that all of the attenuations are weighted equally in calculating the mean. But as can be seen from Eq. (IV-3), the uncertainty decreases as the difference between the two separations increases. Thus, the standard deviation calculated by this method represents an upper bound of the actual uncertainty in the attenuation.

The attenuation was calculated for each value of viscosity using the method of least squares and the mean of all combinations. In each case, the two values of attenuation differed by less than 1%. But we feel that the standard deviation associated with the mean of all combinations was more realistic.

It can be noted that the uncertainty in the separation is by far the biggest source of error. Therefore, to improve these measurements, a method for determining the separation of the transducers more accurately would have to be devised. Toward this end, the separations were corrected using the velocity results. The attenuations were then calculated by the mean of all combinations with these corrected separations. These attenuations were within 1% of the attenuations calculated by the other methods, except for the case of the MS-MH beads of Fig. 11 where the difference was 2.5%. In all but a few cases, the standard deviation was substantially reduced. Thus, the attenuation was calculated by the mean of all combinations. In all but those few cases where the standard deviation was not reduced, the separations were corrected using the velocity results. Reducing the data in this way, we are confident that the attenuations were determined within 3 dB/m, except for a few cases. The attenuations and their uncertainties, corresponding to each fluid viscosity, are listed in Table VII in Chapter IV. They are also listed together with the raw data in Appendix B.

2. Comparison of Results. To determine the validity of the attenuation results, the measurements in the water saturated beads, with no glycerine added, were compared to the results of David Bell (Bell, 1979). His attenuation measurements were given in decibels per wavelength. Converting his results to nepers per meter at 105.0 kHz resulted in the values of 5.45 Np/m and 3.13 Np/m for MS-L and MS-MH size beads, respectively.

The discrepancy in attenuation between Bell's values and those presented in Figs. 10 and 11 was 0.74 Np/m in the first case and 0.73 Np/m in the second. Since this difference was too large to be attributed to experimental error, an effort was made to explain it.

In order to account for the geometrical spreading of the transducers, Bell measured the amplitude decay in water at 120 kHz and the amplitude decay in the sediment at the same frequency. He assumed that the only losses in the water were due to geometrical spreading and that the losses in the sediment were due to geometrical spreading and absorption in the medium. He then assumed that the losses due to geometrical spreading in the sediment were the same as in water, at the same frequency. Therefore, to calculate the attenuation he subtracted the spreading losses, which he determined from his measurements in water, from the total losses (Bell, 1979).

In doing this, he assumed that the geometrical spreading in the water was the same as in the sediment, for measurements taken at the same frequency. But the Rayleigh distance, which is a measure of the distance at which spherical spreading starts, is inversely proportional to the sound speed. Since the sound speed is greater in the sediment than in

the water, the Rayleigh distance is smaller in the sediment than in the water. Also, the distances at which he took his measurements were less than the Rayleigh distance for his transducers, so that in water his amplitude did not vary as 1/r. Therefore, the losses due to geometrical spreading were less in the water than in the sediment. The extra geometrical spreading that was occurring in the sediment was attributed to absorption in the sediment, resulting in a value of attenuation that was too large.

We also compared our measurements in MS-MH beads with those made by Shirley (Bedford, Appendix A, 1982) and Hovem and Ingram (Hovem, 1979). These results are summarized in Table III. Shirley's result, like Bell's, is much higher than ours. We believe that he measured the attenuation in the same way that Bell did. Thus, we feel that his results differ from ours for the same reason that Bell's did.

Hovem and Ingram's results at 100 kHz also differ significantly from ours. If their results at just this one frequency are considered, one might be led to the conclusion that the measured attenuation is very much dependent on the depth of the transducers in the sediment. But if their results at other frequencies in that range are considered, it can be seen that their data exhibit a significant amount of frequency dependence. It is difficult to say whether this exhibited frequency dependence is due to actual physical processes or to scatter in the data. Other frequency dependent measurements need to be taken to investigate this.

Table III: Comparison of Attenuation Results in MS-MH Size Beads.

	Frequency - kHz	Depth - cm	Attenuation - dB/m
Present Study	105.0	12.	20.85
			20.74
			21.61
Bell	120.0	9.	27.10
Shirley	114.0	10.	30.91
Hovem &	60.0	20.	24.86
Ingram	80.0	20.	17.63
	100.0	20.	13.20
	150.0	20.	19.65

There were several assumptions made in our measurements which could affect the validity of the attenuation results. One assumption was that the mechanical coupling between the transducer and the sediment was the same at each separation. To justify this assumption, each time the transducer was moved the sediment-water mixture was vibrated gently for approximately thirty minutes. The mixture was then left undisturbed for another half hour before another measurement was taken. Four or five more readings were then taken over the next three to four hours. Since we found that the amplitude and time delay readings did not change over this period of time, except for small variations attributed to experimental uncertainty, it was assumed that the coupling between the transducer and sediment did not vary.

3. Transient Considerations. From a theoretical viewpoint, it would be desirable to measure the time delay and amplitude using a steady state signal. In this way, we could be confident that the signal had a single frequency. The transient characteristics of the transducers could also be neglected. However, the container holding the sediment has a limited volume. Thus, there will be reflections of the signal from the sides of the container and from the sediment-water interface. To prevent these reflections from interfering with the signal that travels along the direct path between the two transducers, a four cycle pulse was transmitted. The signal was then cut off for several milliseconds so that all the reflections in the sediment would attenuate before a new pulse was transmitted. A photograph of the oscilloscope trace of the transmitted and received signals is shown in Fig. 12. Note that the received signal contains more than four cycles. Since the transducers are being operated at one of their resonant frequencies, they continue to vibrate, or ring, for several cycles after the input signal is turned off.

In this section and the next, an attempt is made to justify treating the pulses as steady state, harmonic signals in analyzing the data and comparing it to the theory. This section discusses the transient effects of the transducers on the signal amplitude. The signal amplitude can also be affected by dispersion. These effects are discussed in the next section.

Since we compared amplitude measurements at different separations to calculate the attenuation, it is assumed that the measured voltage amplitude is linearly proportional to the acoustic

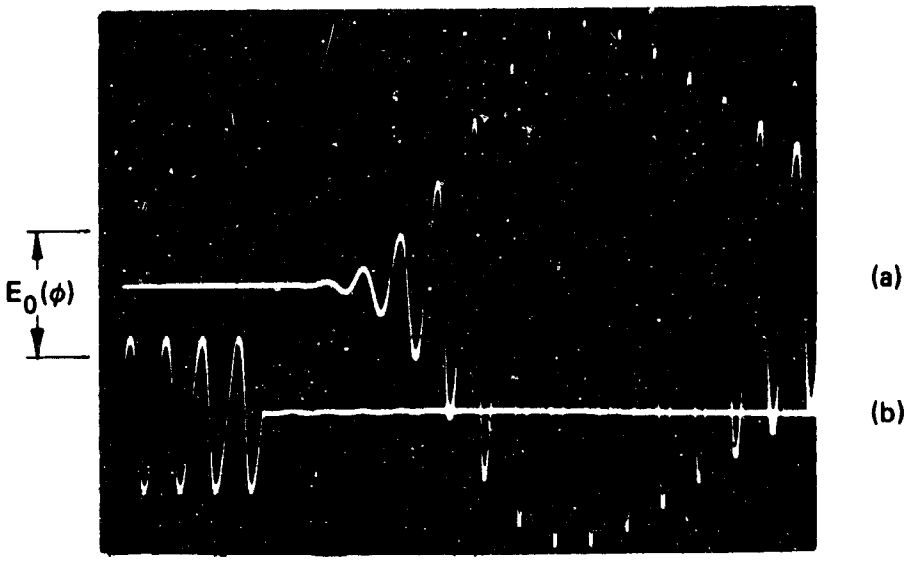

HORIZONTAL SCALE: 20 μs/DIV

VERTICAL SCALE:
(a) RECEIVED SIGNAL – 0.05 V/DIV
(b) TRANSMITTED SIGNAL – 5 V/DIV

SEPARATION: 8.04 cm

FIGURE 12
TRANSMITTING AND RECEIVING PULSES IN SEDIMENTS

pressure amplitude that produced it in the sediment. In order to justify this assumption, consider the block diagram in Fig. 13. The amplitude of the voltage signal put in to the transmitter is denoted by E_i. This produces an acceleration of the transducer face, denoted by u. The signal produced by this motion of the transducer face travels a distance r to the receiver, where it produces a pressure P_0. The receiver converts this pressure signal to an output voltage signal E_0. The phase constant ϕ signifies that the measurements are taken on the fourth cycle. Thus $E_0(\phi)$, shown in Fig. 12, represents the peak-to-peak, voltage amplitude of the fourth cycle of the received signal. The operators L_1, L_2, and L_3 denote linear functions of their arguments.

Our use of the phase constant ϕ deserves some explanation. If T represents the period of one cycle, then the positive and negative peaks of the fourth cycle will correspond to the phases

$$\phi_+ = t_+ - r/c_0 = 3.25\,T$$

and

$$\phi_- = t_- - r/c_0 = 3.75\,T \quad ,$$

respectively. Note that the separation r is the same in each case, so that the difference in the travel times t_+ and t_- is 0.5T. The pressure amplitude of the fourth cycle is then

$$P_0(\phi) = P_0(\phi_+) - P_0(\phi_-) \quad .$$

Since u represents the acceleration of the transducer face, and the phase represented by ϕ spans half of a period, the quantity $u(\phi)$ does not really

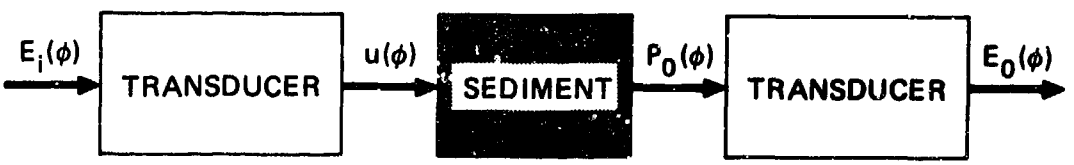

$$u(\phi) = L_1(E_i(\phi)) \qquad P_0(\phi) = \frac{K}{r} e^{-\alpha r} u(\phi) \qquad E_0(\phi) = L_2(P_0(\phi))$$

FIGURE 13
LINEARITY OF THE TRANSDUCERS

ARL:UT
AS-85-260
DRC - GA
3 - 13 - 85

make sense. But in Fig. 13 it represents the quantity

$$u(\phi) = u(\phi_+) - u(\phi_-) \quad .$$

The terms $E_0(\phi)$ and $E_i(\phi)$ have similar meanings.

Consider the two graphs of $E_0(\phi)$ versus $E_i(\phi)$ shown in Fig. 14. These were taken by varying the amplitude of the input voltage, $E_i(\phi)$, and measuring the amplitude of the fourth cycle of the output voltage signal. The graphs were made at the distances r = 10.0 cm and r = 20.0 cm so that the entire range of received amplitudes that were measured in the experiment would be covered. The graphs show that the output amplitude of the fourth cycle, $E_0(\phi)$, is a linear function of the input amplitude E_i. This can be expressed as

$$E_0(\phi) = L_3(E_i(\phi))$$

To calculate the attenuation, it is assumed that the pressure signal decays according to

$$P_0(r,t) = (K/r)\, e^{-\alpha r}\, u(t - r/c_0) \quad ,$$

where K represents an arbitrary constant, and c_0 is the phase velocity. The axial, farfield pressure due to a transient signal in a nonabsorbing, nondispersive medium is

$$P_0(r,t) = (K/r)\, u(t - r/c_0) \quad .$$

To account for the attenuation, the exponential term was incorporated, ad hoc. Taking the attenuation into account in this way is justified because the farfield pressure on the axis for steady state, harmonic

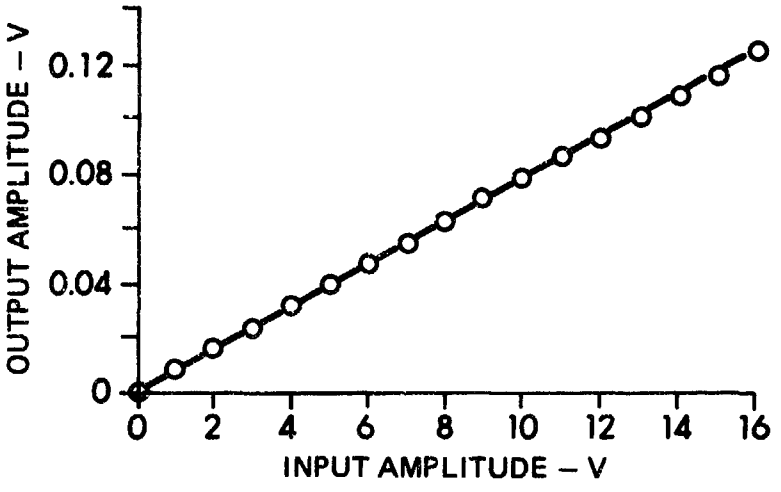

(a) LINEAR AMPLITUDE RELATIONSHIP AT 20 cm

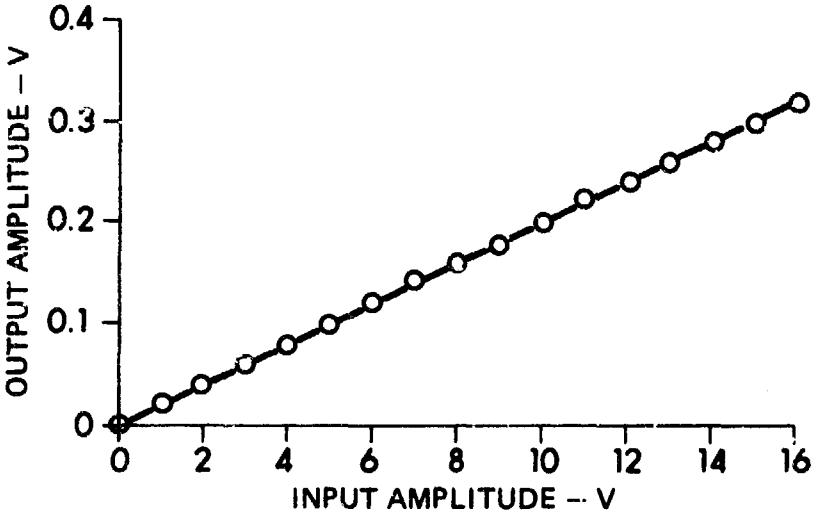

(b) LINEAR AMPLITUDE RELATIONSHIP AT 10 cm

FIGURE 14
INPUT VOLTAGE AMPLITUDE versus OUTPUT VOLTAGE AMPLITUDE OF THE FOURTH CYCLE

ARL:UT
AS-85-261
DRC - GA
3 - 13 - 85

radiation from a baffled piston is given by (Blackstock)

$$P_0(r,t) = (K/r)\, e^{i(\omega t - kr)} \quad .$$

The $e^{-\alpha r}$ term is arrived at in this case by assuming that the wave number k is complex, where α is its imaginary part. Since $u(\phi)$ is a constant, we get

$$P_0(\phi) = (K/r)\, e^{-\alpha r} \quad .$$

Therefore, the assumption used to determine the attenuation,

$$E_0(\phi) = {}^{K}/_{r}\, e^{-\alpha r} \quad , \quad (1)$$

will be valid if $E_0(\phi) = L_2(P_0(\phi))$. (2)

To show that (1) is valid, assume that (2) is true and also that

$$u(\phi) = L_1(E_i(\phi)) \quad .$$

This is the same as assuming that the transducers produce a signal amplitude that is linearly proportional to their signal input, for a given cycle. It therefore follows that:

$$\begin{aligned} E_0(\phi) &= L_2(P_0(\phi)) \\ &= L_2\,[(K/r)\, e^{-\alpha r}\, u(\phi)] \\ &= (K/r)\, e^{-\alpha r}\, L_2(u(\phi)) \\ &= (K/r)\, e^{-\alpha r}\, L_2\{L_1[E_i(\phi)]\} \\ &= (K/r)\, e^{-\alpha r}\, L_3[E_i(\phi)] \\ &= (K'/r)\, e^{-\alpha r}\, E_i(\phi) \end{aligned}$$

where K' is another arbitrary constant. For a fixed r, this shows that $E_0(\phi)$ is linearly proportional to $E_i(\phi)$, which has been demonstrated in

the two graphs of Fig. 14. This result supports the assumption (2). Furthermore, $E_i(\phi)$ is a constant so that (1) directly follows.

4. Effects of Dispersion. In determining the attenuation, the decrease in amplitude with increasing separation was attributed to two causes; spherical spreading and absorption of the medium. In reducing the data, it was assumed that the signal contained only one frequency and that any dispersion could be neglected. But, since the transmitted signal was the product of a sine wave and the difference between two step functions, the signal contained a continuum of frequencies. We justified treating the signal as a pure tone by channeling the signal through a narrow bandpass filter and by making our measurements on the fourth cycle of the signal to minimize transient effects.

Since the signal did contain more than one frequency, dispersion would cause a decrease in amplitude with increasing separation. However, we believe that the effect of dispersion on our measurements is very small. The theory and the measurements predict little change in the phase velocity of the compressional wave of the first type with frequency. Since the received signal is filtered as a further precaution, we would expect the influence of dispersion on the amplitude to be negligible.

To be more confident in this assumption, the attenuation was determined by measuring the amplitudes from three consecutive cycles on the received signal: the third, fourth, and fifth cycles. This was done for three different sets of measurements. The results are shown in Table IV. In each set, the three attenuations are within a standard

deviation. The attenuation of the middle set exhibits the most spread, but even so the spread is still within the estimated uncertainties. Curiously, the standard deviations corresponding to this set are the smallest in the table.

If dispersion was a significant factor, the envelope of the received signal would change shape as the signal propagated through the sediment. This would cause the attenuations measured from amplitudes of different cycles to be distinctly different. Since they are not, we conclude that any error in the attenuation caused by dispersion is negligible within the limits of error of our measuring technique.

Table IV: Comparison of Attenuations and Standard Deviations Measured from Different Cycles of the Same Received Signal.

CYCLE	VISCOSITY -cP	ATTEN - dB/m	STD DEV - dB/m
3	1.33	20.5	3.5
4		20.4	2.9
5		19.5	3.4
3	1.33	20.7	1.7
4		19.0	1.9
5		18.1	2.7
3	2.59	23.6	2.6
4		23.2	2.1
5		23.5	2.4

V. EXPERIMENTAL RESULTS

A. Physical Properties of the Sediment

In order to calculate the wave number using the theory outlined in Chapter II, the physical properties of the saturated sediment needed to be determined. The values of most of these parameters were easily obtained, either by direct measurement or from tables listing material properties, which were found in handbooks and journal articles. Assigning numerical values to some of the other parameters, on the other hand, was not so straightforward.

The physical properties of the solid and fluid constituents were the most easily determined. Glass beads constitute the solid part of the mixture. The density and bulk modulus of glass were found in several sources (Bedford, 1982; Kinsler, 1982). The average grain size, or bead diameter, was measured by Bell from a grain size analysis. The porosity of MS-MH size beads was also determined by Bell (Bell, 1979). These values are listed in Table V.

The properties of the fluid change in the experiment since glycerine is added to the mixture after each set of measurements. The density of the fluid is easily determined by measuring the specific gravity with a hydrometer. Knowing the specific gravity and the temperature, the viscosity was read from a table containing values of viscosity for solutions of varying glycerine-water concentrations (Sheely, 1932). Shirley measured the sound speed in glycerine-water

Table V: Physical Properties and Parameters of Sediment Used in Theoretical Calculations.

PARAMETER	SYMBOL	PRESENT STUDY	BEDFORD	SHIRLEY
Porosity	ϕ	0.365	0.365	0.365
Bead Diameter (cm)	d_m	0.0177	0.018	0.0177
Glass Bulk Modulus ($\times 10^{11}$ dyn/cm^2)	K_s	3.9	4.07	3.5
Glass Density (g/cm^3)	ρ_s	2.5	2.5	2.5
Frame Bulk Modulus (dyn/cm^2)	K_b	8.0×10^7	5.8×10^9	8.0×10^7
Frame Shear Modulus (dyn/cm^2)	μ_b	8.0×10^7	5.8×10^9	8.0×10^7
Comp. Log Decrement	δ_c	0.1	0.15	0.1
Shear Log Decrement	δ_s	0.1	0.15	0.1
Permeability ($\times 10^{-7}$ cm^2)	B_0	3.8	2.48	2.64
Kozeny-Carman Constant	k_0	2.76	4.23	3.98
Depth in Sediment (cm)		12	20	10

solutions with varying concentrations of glycerine (Bedford, Appendix A, 1982). From this data, and values of density and viscosity at 20°C found in the CRC Handbook, he was able to determine the bulk modulus as a function of viscosity for concentrations up to 32% glycerine, by weight. But since his measurements were taken at room temperature, which is closer to 25°C, we adjusted his measurements so that the bulk modulus values corresponded to viscosity values at 25°C. His results were then projected to include glycerine concentrations up to 40%. The results of this procedure are shown in Table VI. This extrapolation of his data is questionable at best, but there was not enough time to repeat the measurements. These adjustments produce only slight changes in the theoretical predictions. At some point in the future it would be desirable to redo and hopefully repeat Shirley's measurements.

The properties of the solid matrix are more difficult to determine. With all of the other properties defined, these properties were chosen so that the theoretical predictions and the experimental data agreed for the case of pure water. Once this agreement was satisfied, we were able to show that the Biot-Stoll theory predicted the same change in attenuation and phase velocity that was indicated by the experimental data as the viscosity of the pore fluid was increased.

Four of these properties were the real and imaginary parts of the bulk and shear moduli of the drained glass beads. Hovem and Ingram (Hovem, 1979), Shirley (Bedford, Appendix A, 1982), and Bedford (Bedford, 1984) chose the real parts of both of these moduli so that there was agreement between the theory and compressional velocity

Table VI: Physical Properties of Fluid Used in Theoretical Calculations.

VISCOSITY η - cP	FLUID DENSITY ρ_f - g/cm^3	FLUID BULK MODULUS K_f - $\times 10^{10}$ dyn/cm^2
0.893	0.9971	2.175
1.0	1.0080	2.284
1.2	1.0242	2.442
1.4	1.0373	2.574
1.6	1.0483	2.683
1.8	1.0576	2.781
2.0	1.0654	2.867
2.2	1.0723	2.943
2.4	1.0785	3.012
2.6	1.0840	3.075
2.8	1.0887	3.128

data. Bedford made theoretical comparisons with Hovem and Ingram's data and his choices of the parameters are very similar to Hovem and Ingram's.

Bedford had good agreement between theory and data for

$$K_b = \mu_b = 5.8 \times 10^9 \ dyn/cm^2 \quad .$$

But Hovem and Ingram's measured compressional velocity at 100 kHz, 1922 m/s, is considerably higher than ours for the pure water case, 1830 m/s. This is presumably because their measurements were made 8 cm deeper in the sediment than ours were. As a result, their choice of K_b and μ_b produced theoretical velocities that were too large for our data. But the theoretical attenuations produced by this choice compared well with our data. Shirley's measured velocity, at 114 kHz with pure water as the pore fluid, agreed quite well with our results. It should be noted that our measurements were taken at similar depths. His choice for the two moduli was

$$K_b = \mu_b = 8.0 \times 10^7 \ dyn/cm^2 \quad .$$

This choice produced theoretical velocities that agreed quite well with our data. The disparity between these two sets of values suggests that the properties of the sediment change drastically with increasing depth in the sediment.

We used Shirley's values for the bulk and shear moduli, even though the theoretical attenuations they produced were much too high. This discrepancy, which was the result of differences in experimental technique and data reduction, was discussed in Section IV.B.2. In order

to achieve a good fit between the theory and the experimental data for the attenuation case, we had to choose other parameters differently from Shirley.

The imaginary parts of the bulk and shear moduli of the granular matrix are the terms that take into account the losses at the grain-to-grain contacts. From our experience, these parameters have negligible effect on the compressional velocity, and only a slight effect on the attenuation. In the literature, these two parameters have been related to their real counterparts by two other parameters, the compressional and shear logarithmic decrements, δ_c and δ_s, respectively. The relationships defining these parameters are

$$K_b' = \delta_c K_b/\pi \qquad \text{and} \qquad \mu_b' = \delta_s \mu_b/\pi$$

where a primed variable denotes the imaginary part of the modulus and an unprimed varible denotes the real part. Our choices of these variables are listed in Table V.

The last parameter to be chosen was the permeability. Bell measured this quantity directly for four sizes of glass beads and three different sands (Bell, 1979). For the MS-MH size beads he measured the permeability to be $B_0 = 1.70 \times 10^{-7}$ cm^2. The permeability is related to an empirical parameter, the Kozeny-Carman constant, k_0, by the relation (Bell, 1979)

$$B_0 = \frac{d_m^2 \phi^3}{36 k_0 (1-\phi)^2} \quad .$$

Bell's value for B_0 corresponded to $k_0 = 6.17$. Hovem and Ingram chose $k_0 = 4.23$ so that $B_0 = 2.48 \times 10^{-7}$ cm^2. Shirley used $k_0 = 3.98$ so that $B_0 = 2.64 \times 10^{-7}$ cm^2. We found good correlation between theory and data by choosing $B_0 = 3.7 \times 10^{-7}$ cm^2. This corresponded to $k_0 = 2.83$. This was within the range of values in the data presented by Stoll (Stoll, 1974) and also within the range of values measured by Bell for several sands and sizes of glass beads.

Table V summarizes the values of the physical properties and parameters used in the present study, and also those chosen by Bedford (Bedford, 1984) and Shirley (Bedford, Appendix A, 1982). In Fig. 15 our data are compared with the theory with Bedford's, Shirley's, and our choices of the parameters.

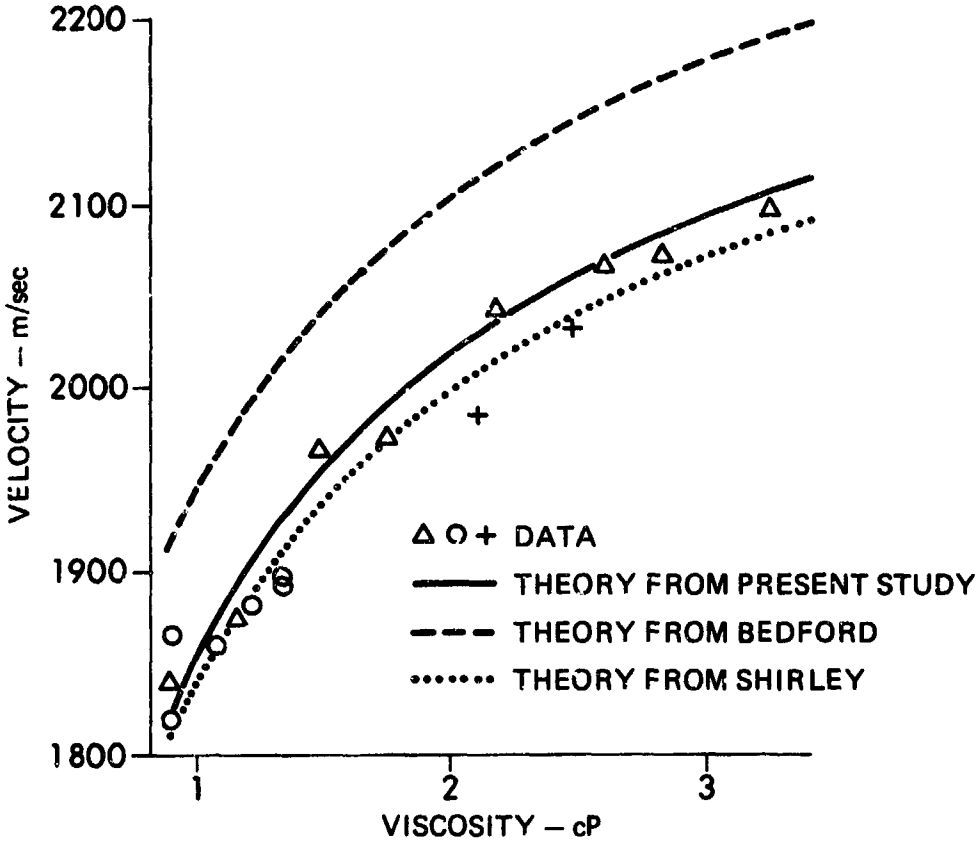

(a) PHASE VELOCITY

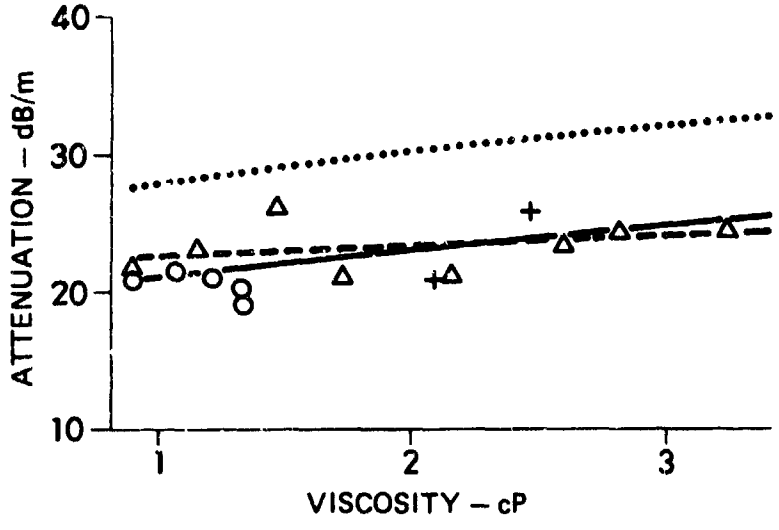

(b) ATTENUATION

FIGURE 15
COMPARISON OF BIOT THEORY TO DATA

ARL:UT
AS-85-337
DRC - GA
3 - 28 - 85

Table VII: Velocity and Attenuation in MS-MH Beads with Variable Fluid Properties.

VISCOSITY η - cP	VELOCITY c_0 - m/sec	STD. DEV. σ_{c_0} - m/sec	ATTENUATION α - dB/m	STD. DEV. σ_α -dB/m
	BATCH 1			
0.89	1820.0	23.6	20.7	4.1
0.89	1869.7	9.0	20.7	1.1
1.07	1861.3	6.8	21.3	2.2
1.22	1878.9	2.6	21.0	3.1
1.33	1893.3	4.2	20.4	2.9
1.33	1898.6	5.7	19.0	1.9
	BATCH 2			
0.89	1839.4	15.2	21.7	2.5
1.15	1873.8	8.7	23.1	2.2
1.48	1966.7	9.4	26.0	3.6
1.74	1973.3	8.9	20.9	2.8
2.16	2044.1	7.3	21.0	1.7
2.59	2067.5	9.2	23.2	2.1
2.81	2074.5	13.0	24.3	1.4
3.23	2098.8	12.1	24.3	2.2
	DILUTING BATCH 2			
2.46	2034.7	8.2	26.0	1.7
2.09	1986.6	3.6	20.8	1.6

repeatability of the results. The results for the three cases agree reasonably well with each other and also with the theoretical curves. The figures demonstrate that these experimental results are repeatable within the estimated uncertainties, especially in the phase velocity case. The larger amount of scatter, and the larger uncertainties, in the attenuation results suggest that further improvements can be made in that measurement technique. One suggestion would be to design a bracket that would hold the transducer mount and guide it straight into the sediment while it was being repositioned. This would probably be the easiest and least expensive way to reduce the most significant cause of experimental error, that due to uncertainty in the separation measurements.

The sediment is disturbed each time a transducer is repositioned to take travel time and amplitude measurements at a new separation. It is also disturbed after each set of measurements, when the pore fluid is circulated and glycerine is added to it to modify its properties. The sample is also vibrated during this process, so it is disturbed even more. Any such disturbance of the sediment would affect the packing of the individual grains. There has been some concern that the acoustic propagation through sediments was very dependent upon this packing. If the propagation were very dependent on the packing, it would be very difficult to repeat the results. The repeatability of our results suggests that the propagation is not very dependent on the packing of the individual grains, at least in the case of compressional wave propagation. This is fortunate, because it would be very difficult and

tedious to control the packing of glass beads and sediments of sizes this small. The good correlation between the data and their least squares fits, shown in Figs. 8 through 11, also supports this conclusion. We conjecture that the actual packing of the glass beads, or sediment, would have more of an effect on shear wave results.

Problems associated with the coupling between the transducers and the sediment could also affect the repeatability of the results. When there is good coupling between the transducer and the sediment, a large amount of energy is transferred from the transducer to the sediment in the case of the transmitter, and vice-versa for the receiver. Due to a difference of impedances between the piezoelectric element and the sediment, all of the energy will not be transmitted, but if the coupling is good, the amount of energy transferred will be a maximum. If there is not good coupling between the transducers and the sediment, the measured voltage amplitude will be less than the amplitude of a signal produced by good coupling. Since the radiating surface of our transducers was very much larger than the diameter of the glass beads, the coupling between the transducers and the sediment was always good and the energy transferred from the transducer to the sediment, and vice-versa, was always adequate. Several observations support this conclusion. First, a strong signal was received immediately after the transducer was inserted. Nevertheless, the entire sample was gently vibrated for twenty to thirty minutes, and then the sediment set undisturbed for another twenty to thirty minutes more before a

measurement was taken. The signal was monitored for at least three more hours before the transducer was repositioned. During this period, the time delay and amplitude readings varied only by amounts attributed to instrumental uncertainties. The good correlation between the data and the least square fits also supports the conclusion that there was no appreciable variation in the coupling between the transducer and the sediment during the period the readings were being taken.

In the discussion of experimental errors in the phase velocity and attenuation, no mention has been made of the accuracy with which the viscosity was determined. As mentioned in Section III.D. on the preparation of the sediment, the viscosity was determined by measuring the specific gravity of the pore fluid using a hydrometer, and then reading the value of viscosity from a table containing the specific gravity and viscosity of varying concentrations of glycerine-water solutions. The error in the viscosity is difficult to estimate. Most of this error is believed to be due to the variations of the temperature in the room where the experiment was performed. The temperature in the laboratory was usually between 24°C and 26°C, so most pore fluid viscosities were determined assuming that the room temperature was 25°C. The theoretical predictions were made assuming that the temperature was 25°C. For the most part this produced acceptable results, especially for the triangle data points of Fig. 15. Luckily, the laboratory temperature stayed consistently between 24°C and 26°C during the time these data points were taken.

For the other measurements, the temperature varied between 22°C and 26°C. This 4° variation in temperature can produce a change in viscosity of over 10%. Not only did this affect the accuracy at which the viscosity was determined, but it also affected the velocity and attenuation results, which are temperature and viscosity dependent. Therefore temperature variation could be a source of some of the uncertainties in the attenuation and velocity measurements. In future investigations, it would be advisable to perform similar experiments in constant temperature environments.

Taking the experimental uncertainties that have been discussed into account, the Biot-Stoll theory appears to adequately describe the effects of the fluid properties on acoustic wave propagation in saturated sediments, at least for compressional waves of the first type. Similar experiments investigating shear wave propagation and the compressional wave of the second type need to be performed. We observe that these types of measurements are more difficult to make.

VI. DISCUSSION AND CONCLUSIONS

The purpose of the work presented here was to design and perform an experiment that would examine the dependence of compressional wave propagation in fluid saturated sands on the properties of the pore fluid. Since this dependence was predicted by the Biot-Stoll equations, it was hoped that these measurements would be a critical test of the theory. Experiments of this type had already been performed by Shirley (Bedford, Appendix A, 1982), and then later by Elliot (Bedford, 1982). However, due to large scatter in the experimental data, no definite conclusions could be made about their results.

The measurement techniques used in this investigation were refinements of techniques developed and used by Shirley (Shirley, 1977; Bedford, 1982), Bell (Bell, 1979), and Elliot (Bedford, 1982). All three of these investigators measured the phase velocity and attenuation of both compressional and shear waves. After making a few modifications in their technique, new measurements have been taken and shown to be repeatable. The main improvement over the earlier work resulted from redesigning the compressional wave transducers so that the geometrical spreading and directivity could be predicted. With this improvement, spherical spreading was established at the separations at which these measurements were taken. Thus, the losses due to geometrical spreading were accurately accounted for when analyzing the data. It was also possible to make reasonable estimates of the experimental

uncertainties. Because of the paramount difficulties involved in making repeatable shear wave measurements, these measurements were postponed.

Taking the experimental uncertainty into account, the data are in good agreement with the theory. Since parameters were chosen so that the theoretical values were in agreement with the experimental results for the case of pure water, the present results indicate that the theory predicts the same trend in attenuation and phase velocity, with changing properties of the pore fluid, that is exhibited by the data. But since there was also good agreement with the fresh water velocity results of Shirley, taken at approximately the same depth, the choices of the real parts of the bulk and shear moduli appear to be reasonable estimates of these parameters. Further experimental investigations examining the depth and frequency dependence of compressional wave propagation in sediments are needed to support this conclusion.

These compressional wave results, on the other hand, do not give a strong indication of the values of the imaginary parts of these moduli. To get more reliable estimates of these parameters, shear wave measurements in the same size glass beads need to be taken. Shear wave velocity measurements are easily accessible with only a modest investment in time and equipment.

On the other hand, it is believed that shear wave attenuation measurements would be much more difficult. One of these difficulties, especially in the glass beads, would be the coupling between the transducer and the sediment. Once this problem has been surmounted,

establishing the directivity of shear wave transducers would also be tedious and time consuming. However, if a procedure similar to the one described here were used, this would be an essential step. Only in this way could an experimenter be sure that the amplitude decay being measured was due to the increased separation of the transducers, and not their directivity.

It would also be important to establish which part of the total losses would be due to the geometrical spreading of the transducers. This would probably be the most difficult of the three tests to conduct. The most common type of transducers used in experimental shear wave propagation studies are shear wave bender elements. The problem would be to locate a lossless, elastic medium in which the bender elements would work so that the losses due to the spreading of the signal could be determined.

Fortunately for our case, Rayleigh had already solved for the farfield pressure produced by a moving piston in a rigid baffle. All that we needed to do was verify that this model adequately predicted the measured characteristics of our transducers and that our measurements were taken in the farfield. It would be helpful if a similar model could be derived to describe the stress field or the displacement field of shear bender elements. With a model of this type, establishing the characteristics of this type of transducer would be simpler.

APPENDIX A

COMPUTER PROGRAM

The FORTRAN program presented here is a simple algorithm that calculates the phase velocity and attenuation of sound in saturated sediments using the Biot-Stoll theory. The program solves the quadratic formula (II-3), from Chapter II for different values of viscosity, density, and bulk modulus of the pore fluid. The fluid properties used in this study are shown in Table VI of Chapter V and were fed to the program by the input data file DATAIN. The physical properties of the solid and solid matrix were either entered interactively or in the DATA statement. The values of these properties are listed in Table V of Chapter V.

The experimental results of Table VII were also entered into the program through DATAIN. The program plots the theoretical and experimental results, shown in Fig. 15, so that they can be compared. A list of the parameters used in the program, along with their corresponding FORTRAN and mathematical symbols, is given in Table VIII, followed by a listing of the FORTRAN program BIVO.

Table VIII: Parameters Used in FORTRAN program BIVO.

PARAMETER	MATH SYMBOL	FORTRAN SYMBOL
Pore Size	a_p	A
Virtual Drag Coefficient	b	B
Virtual Mass Coefficient	c	C
Biot Coefficients	C	CB
(complex)	H	HB
	M	MB
(real)	D	D
Permeability	B_0	BO
Grain Diameter	d_m	DM
Porosity	ϕ	PHI
Solid Density	ρ_s	ROS
Fluid Density	ρ_f	ROF
Mixture Density	ρ	RO
	ρ_c	ROC
Viscosity	η	ETA, VISC VISC2, VISC3
Phase Velocity	c_0	CPHASE C1, C2, C3

PARAMETER	MATH SYMBOL	FORTRAN SYMBOL
Attenuation	α	ATTEN, ALPHA ALPHA2, ALPHA3
Frequency	f	FR
Angular Frequency	ω	OMEGA
Fluid Bulk Modulus	K_f	KBF
Solid Bulk Modulus	K_s	KBS
Bulk Modulus of Drained Solid Matrix (complex)	K_b	KBB
Shear Modulus of Drained Solid Matrix (complex)	μ	MUB
Compressional Logarithmic Decrement	δ_c	DELC
Shear Logarithmic Decrement	δ_s	DELS

```
C  PROGRAM BIVD CALCULATES AND PLOTS PHASE VELOCITY AND ATTENUATION
C    OF SOUND IN BIOT MATERIALS AS A FUNCTION OF VISCOSITY OF THE PORE FLUID.
C  PROGRAM CALLS THE SPECIAL FUNCTIONS MMKELO AND MMKELD IN THE IMSL LIBRARY.
C  PROGRAM READS FROM FILE DATAIN AND WRITES TO FILE DATOUT.
C  OTHER INPUT IS ENTERED INTERACTIVELY.
C  COMMON BLOCKS ARE ORGANIZED AS FOLLOWS:
C    /ATVEL/  CONTAINS THE ARRAYS USED TO PLOT THE THEORETICAL PREDICTIONS.
C    /EXPDAT/, /EXPDAT2/, /EXPDAT3/ CONTAIN THE ARRAYS THAT CONTAIN
C    THE EXPERIMENTAL DATA TO BE PLOTTED.
C
C
C
      PROGRAM BIVD(INPUT,OUTPUT,DATAIN,PLOT,DATOUT,
     $TAPE5=DATAIN,TAPE3=DATOUT)
      REAL KI,KR,KBS,KBF(20),ROF(20)
      COMPLEX I,KBB,MUB,HB,MB,CB,T,F,K,A1,A2,A3,A4
      COMMON /ATVEL/ ATTEN(20),CPHASE(20),ETA(20),N
      COMMON /EXPDAT/ VISC(20),C1(20),ALPHA(20),ND
      COMMON /EXPDAT2/ VISC2(20),C2(20),ALPHA2(20),ND2
      COMMON/EXPDAT3/ VISC3(20),C3(20),ALPHA3(20),ND3
      DATA PHI,ROS,DM/.365,2.50,.0177/
      I=CMPLX(0.,1.)
      PRINT*,"ENTER REAL PARTS OF BULK AND SHEAR MODULI, KBB AND MUB"
      READ*,XKB,XMU
      PRINT*,"ENTER LOG DECREMENTS, DELC AND DELS"
      READ*, DELC,DELS
      PRINT*,"ENTER KBS AND BO"
      READ*,KBS,BO
C
C  IMAGINARY PARTS OF BULK AND SHEAR MODULI
C  IN TERMS OF REAL PARTS AND LOG DECREMENTS.
C
      XKBP=DELC*XKB/3.14159
      XMUP=DELS*XMU/3.14159
      KBB=CMPLX(XKB,XKBP)
      MUB=CMPLX(XMU,XMUP)
      PRINT*,"INPUT FREQUENCY IN HERTZ"
      READ*,FREQ
      OMEGA=2.*3.14159*FREQ
      READ(5,*)N
```

```
      WRITE(3,39)
C
C  PROPERTIES OF FLUID ARE READ IN DO LOOP.
C  ATTENUATION AND PHASE VELOCITY ARE CALCULATED
C  FOR EACH VALUE OF VISCOSITY READ IN.
C
      DO 30 J=1,N
        READ(5,*) ETA(J), ROF(J), KBF(J)
        ETA(J)=ETA(J)/100.
        D=KBS*(1 +PHI*(KBS/KBF(J)-1. ))
        MB=((KBS-KBB)**2)/(D-KBB)+KBB+4. *MUB/3.
        MB=KBS*KBS/(D-KBB)
        CB=KBS*(KBS-KBB)/(D-KBB)
        RO=(1. -PHI)*ROS+PHI*ROF(J)
        A=PHI*D*1/3. /(1. -PHI)
        X=A*(OMEGA*ROF(J)/ETA(J))**0.5
        CALL MMKELO(X,BER,BEI,XKER,XKEI,IER)
        CALL MMKELD(X,BERP,BEIP,XKERP,XKEIP,IER)
        T=CMPLX(BERP,BEIP)/CMPLX(BER,BEI)
        F=X*T/4. /(1. -2. *T/I/X)
        FI=AIMAG(F)
        FR=REAL(F)
        B=PHI*PHI*ETA(J)*FR/BO
        C=PHI*PHI*ETA(J)*FI/OMEGA/BO
        ROC=ROF(J)/PHI+C/(PHI*PHI)
        A1=CB*CB-MB*HB
        A2=OMEGA*OMEGA*(RO*MB+ROC*HB-2. *ROF(J)*CB)
     &  -I*OMEGA*HB*B/PHI/PHI
        A3=B*RO*I*OMEGA**3. /PHI**2. +OMEGA**4. *(ROF(J)*ROF(J)-RO*ROC)
        A4=CSQRT(A2*A2-4. *A1*A3)
        K=CSQRT((-A2+A4)/(2. *A1))
        KI=AIMAG(K)
        KR=REAL(K)
        ATTEN(J)=-KI*100. *8. 686
        CPHASE(J)=OMEGA/KR/100.
        ETA(J)=ETA(J)*100.
        WRITE(3,40) ETA(J),ROF(J),KBF(J),ATTEN(J),CPHASE(J)
 30   CONTINUE
C
C  EXPERIMENTAL DATA TO BE PLOTTED IS READ IN
```

```
C   THE FOLLOWING THREE DO LOOPS.
C
      READ(5,*)ND
      DO 35 J=1,ND
        READ(5,*) VISC(J),C1(J),ALPHA(J)
        ALPHA(J)=ALPHA(J)*8.686
 35   CONTINUE
      READ(5,*)ND2
      DO 38 J=1,ND2
        READ(5,*) VISC2(J),C2(J),ALPHA2(J)
        ALPHA2(J)=ALPHA2(J)*8.686
 38   CONTINUE
      READ(5,*)ND3
      DO 42 J=1,ND3
        READ(5,*) VISC3(J),C3(J),ALPHA3(J)
        ALPHA3(J)=ALPHA3(J)*8.686
 42   CONTINUE
      WRITE(3,45) KBS,BO
      WRITE(3,50) XKB,XMU
      WRITE(3,55) DELC,DELS
      WRITE(3,60) FREQ
      CALL MYPLOT
      STOP
 39   FORMAT (6X,"VISC",7X,"ROF",12X,"KBF",7X,"ATTEN-DB/M",
     $5X,"CPHASE-M/S",//)
 40   FORMAT(5X,2(F6.4,5X),E10.3,5X,F10.2,5X,F10.2)
 45   FORMAT(//,5X,"KBS=",E10.3,5X,"BO=",E10.3)
 50   FORMAT (5X,"XKB=",E10.3,5X,"XMU=",E10.3)
 55   FORMAT (5X,"DELC=",F9.2,5X,"DELS=",F5.2)
 60   FORMAT (5X,"FREQ=",F10.1," HZ")
      END
```

```
      SUBROUTINE MYPLOT
C
C  MYPLOT IS A SUBROUTINE THAT CREATES A PLOTFILE.
C  IT USES OTHER SUBROUTINES THAT ARE IN THE ARL LIBRARY.
C
      COMMON/ATVEL/ ATTEN(20),CPHASE(20),ETA(20),N
      COMMON/EXPDAT/ VISC(20),C(20),ALPHA(20),ND
      COMMON /EXPDAT2/ VISC2(20),C2(20),ALPHA2(20),ND2
      COMMON/EXPDAT3/ VISC3(20),C3(20),ALPHA3(20),ND3
      DATA XSTRT,XEND,XLEN/0.8,3.4,6.0/
      DATA VSTRT,VEND,YLEN,ASTRT,AEND/1800.,2100.,6.0,0.0,40./
      DX=(XEND-XSTRT)/XLEN
      DA=(AEND-ASTRT)/YLEN
      DV=(VEND-VSTRT)/YLEN
      CALL PLTLFN(4LPLOT)
      CALL PLTORG(.5,.5)
      CALL PLTAXIS(0.,0.,XLEN,0.,XSTRT,XEND,.2,9HVISC (CP),-9,1)
      CALL PLTAXIS(0.,0.,YLEN,90.,ASTRT,AEND,10.,12HATTEN (DB/M),12,1)
      CALL PLTDATA(ETA,ATTEN,N,0,0,XSTRT,DX,ASTRT,DA,.08)
      CALL PLTDATA(VISC,ALPHA,ND,-1,1,XSTRT,DX,ASTRT,DA,.08)
      CALL PLTDATA(VISC2,ALPHA2,ND2,-1,2,XSTRT,DX,ASTRT,DA,.08)
      CALL PLTDATA(VISC3,ALPHA3,ND3,-1,3,XSTRT,DX,ASTRT,DA,.08)
      CALL PLTEND(8.5)
      CALL PLTLFN(4LPLOT)
      CALL PLTORG(.5,.5)
      CALL PLTAXIS(0.,0.,XLEN,0.,XSTRT,XEND,.2,9HVISC (CP),-9,1)
      CALL PLTAXIS(0.,0.,YLEN,90.,VSTRT,VEND,50.,14HVELOCITY (M/S),14,1)
      CALL PLTDATA(ETA,CPHASE,N,0,0,XSTRT,DX,VSTRT,DV,.08)
      CALL PLTDATA(VISC,C,ND,-1,1,XSTRT,DX,VSTRT,DV,.08)
      CALL PLTDATA(VISC2,C2,ND2,-1,2,XSTRT,DX,VSTRT,DV,.08)
      CALL PLTDATA(VISC3,C3,ND3,-1,3,XSTRT,DX,VSTRT,DV,.08)
      CALL PLTEND(8.5)
      RETURN
      END
```

APPENDIX B

EXPERIMENTAL DATA

BEAD TYPE: MS-MH

FREQUENCY: 105.0 kHz VISCOSITY: 0.893 cP

AMPLITUDE - volts	TIME - µs	SEPARATION - cm
0.3720	65.88	5.65
0.2690	77.63	7.65
0.2004	88.98	9.65
0.1570	100.12	11.65
0.1300	112.07	13.65
0.1074	121.38	15.65
0.0892	133.23	17.65
0.0777	142.31	19.65

VELOCITY: 1820.0 m/s

STANDARD DEVIATION OF VELOCITY: 23.6 m/s

LINEAR CORRELATION COEFFICIENT: 0.9995

ATTENUATION: 2.38 Np/m

STANDARD DEVIATION OF ATTENUATION: 0.47 Np/m

BEAD TYPE: MS-MH

FREQUENCY: 105.0 kHz VISCOSITY: 0.893 cP

AMPLITUDE - volts	TIME - µs	SEPARATION - cm
0.1286	62.21	5.65
0.0907	73.60	7.65
0.0690	84.04	9.65
0.0542	94.83	11.65
0.0440	105.90	13.65
0.0366	115.97	15.65
0.0309	126.98	17.65
0.0266	137.16	19.65

VELOCITY: 1869.7 m/s

STANDARD DEVIATION OF VELOCITY: 9.0 m/s

LINEAR CORRELATION COEFFICIENT: 0.9999

ATTENUATION: 2.38 Np/m

STANDARD DEVIATION OF ATTENUATION: 0.12 Np/m

BEAD TYPE: MS-MH

FREQUENCY: 105.0 kHz VISCOSITY: 1.07 cP

AMPLITUDE - volts	TIME - µs	SEPARATION - cm
0.1310	61.69	5.65
0.0912	72.61	7.65
0.0696	82.62	9.65
0.0547	93.72	11.65
0.0441	104.37	13.65
0.0372	115.05	15.65
0.0310	126.53	17.65
0.0268	136.68	19.65

VELOCITY: 1861.3 m/s

STANDARD DEVIATION OF VELOCITY: 6.8 m/s

LINEAR CORRELATION COEFFICIENT: 0.9999

ATTENUATION: 2.46 Np/m

STANDARD DEVIATION OF ATTENUATION: 0.25 Np/m

BEAD TYPE: MS-MH

FREQUENCY: 105.0 kHz VISCOSITY: 1.22 cP

AMPLITUDE - volts	TIME - μs	SEPARATION - cm
0.1325	61.17	5.65
0.0928	71.66	7.65
0.0702	82.34	9.65
0.0550	92.80	11.65
0.0448	103.58	13.65
0.0370	114.31	15.65
0.0321	124.96	17.65
0.0270	135.59	19.65

VELOCITY: 1878.9 m/s

STANDARD DEVIATION OF VELOCITY: 2.6 m/s

LINEAR CORRELATION COEFFICIENT: 1.0000

ATTENUATION: 2.42 Np/m

STANDARD DEVIATION OF ATTENUATION: 0.36 Np/m

BEAD TYPE: MS-MH

FREQUENCY: 105.0 kHz VISCOSITY: 1.33 cP

AMPLITUDE - volts	TIME - µs	SEPARATION - cm
0.1280	60.74	5.66
0.0916	71.00	7.66
0.0697	81.30	9.63
0.0544	92.02	11.65
0.0445	102.42	13.62
0.0375	112.98	15.61
0.0320	123.17	17.61
0.0274	134.40	19.63

VELOCITY: 1898.6 m/s

STANDARD DEVIATION OF VELOCITY: 5.7 m/s

LINEAR CORRELATION COEFFICIENT: 1.0000

ATTENUATION: 2.18 Np/m

STANDARD DEVIATION OF ATTENUATION: 0.22 Np/m

BEAD TYPE: MS-MH

FREQUENCY: 105.0 kHz VISCOSITY: 1.33 cP

AMPLITUDE - volts	TIME - µs	SEPARATION - cm
0.1310	60.97	5.67
0.0920	71.20	7.64
0.0707	81.59	9.62
0.0546	92.60	11.64
0.0443	103.14	13.63
0.0370	113.47	15.62
0.0316	124.25	17.65
0.0275	134.22	19.58

VELOCITY: 1893.3 m/s

STANDARD DEVIATION OF VELOCITY: 4.2 m/s

LINEAR CORRELATION COEFFICIENT: 1.0000

ATTENUATION: 2.35 Np/m

STANDARD DEVIATION OF ATTENUATION: 0.33 Np/m

BEAD TYPE: MS-1H

FREQUENCY: 105.0 kHz VISCOSITY: 0.893 cP

AMPLITUDE - volts	TIME - µs	SEPARATION - cm
0.1193	63.61	6.0
0.0890	73.32	8.0
0.0654	85.83	10.0
0.0526	95.53	12.0
0.0430	106.16	14.0
0.0352	117.32	16.0
0.0300	128.65	18.0
0.0258	139.50	20.0

VELOCITY: 1839.4 m/s

STANDARD DEVIATION OF VELOCITY: 15.2 m/s

LINEAR CORRELATION COEFFICIENT: 0.9998

ATTENUATION: 2.50 Np/m

STANDARD DEVIATION OF ATTENUATION: 0.29 Np/m

BEAD TYPE: MS-MH

FREQUENCY: 105.0 kHz VISCOSITY: 1.15 cP

AMPLITUDE - volts	TIME - µs	SEPARATION - cm
0.1218	62.70	6.1
0.0868	73.42	8.1
0.0654	84.32	10.1
0.0516	94.61	12.0
0.0427	104.86	14.0
0.0354	115.86	16.0
0.0299	126.78	18.0
0.0256	136.53	20.0

VELOCITY: 1873.8 m/s

STANDARD DEVIATION OF VELOCITY: 8.7 m/s

LINEAR CORRELATION COEFFICIENT: 0.9999

ATTENUATION: 2.66 Np/m

STANDARD DEVIATION OF ATTENUATION: 0.25 Np/m

BEAD TYPE: MS-MH

FREQUENCY: 105.0 kHz VISCOSITY: 1.48 cP

AMPLITUDE - volts	TIME - µs	SEPARATION - cm
0.1190	62.02	6.05
0.0850	72.65	8.09
0.0646	82.73	10.00
0.0518	92.36	12.05
0.0416	102.45	14.02
0.0340	112.99	16.03
0.0280	123.55	18.05
0.0238	132.91	20.00

VELOCITY: 1966.7 m/s

STANDARD DEVIATION OF VELOCITY: 9.4 m/s

LINEAR CORRELATION COEFFICIENT: 0.9999

ATTENUATION: 2.99 Np/m

STANDARD DEVIATION OF ATTENUATION: 0.41 Np/m

BEAD TYPE: MS-MH

FREQUENCY: 105.0 kHz VISCOSITY: 1.74 cP

AMPLITUDE - volts	TIME - µs	SEPARATION - cm
0.1193	61.24	6.06
0.0870	71.06	8.02
0.0649	81.55	10.02
0.0514	91.70	12.05
0.0420	102.19	14.05
0.0350	112.25	16.02
0.0304	121.78	18.02
0.0258	131.66	20.00

VELOCITY: 1973.3 m/s

STANDARD DEVIATION OF VELOCITY: 8.9 m/s

LINEAR CORRELATION COEFFICIENT: 0.9999

ATTENUATION: 2.41 Np/m

STANDARD DEVIATION OF ATTENUATION: 0.33 Np/m

BEAD TYPE: MS-MH

FREQUENCY: 105.0 kHz VISCOSITY: 2.25 cP

AMPLITUDE - volts	TIME - µs	SEPARATION - cm
0.1180	61.42	6.06
0.0860	70.69	8.03
0.0645	80.80	10.06
0.0515	90.20	12.00
0.0419	100.52	14.04
0.0348	110.25	16.03
0.0298	119.87	18.00
0.0258	129.16	20.00

VELOCITY: 2044.1 m/s

STANDARD DEVIATION OF VELOCITY: 7.3 m/s

LINEAR CORRELATION COEFFICIENT: 1.0000

ATTENUATION: 2.42 Np/m

STANDARD DEVIATION OF ATTENUATION: 0.19 Np/m

BEAD TYPE: MS-MH

FREQUENCY: 105.0 kHz VISCOSITY: 2.59 cP

AMPLITUDE - volts	TIME - µs	SEPARATION - cm
0.1180	60.55	6.02
0.0843	70.45	8.03
0.0649	79.30	10.01
0.0500	89.72	12.04
0.0410	98.97	13.99
0.0336	109.21	16.04
0.0285	118.76	18.03
0.0250	127.41	19.85

VELOCITY: 2067.5 m/s

STANDARD DEVIATION OF VELOCITY: 9.2 m/s

LINEAR CORRELATION COEFFICIENT: 0.9999

ATTENUATION: 2.67 Np/m

STANDARD DEVIATION OF ATTENUATION: 0.24 Np/m

BEAD TYPE: MS-MH

FREQUENCY: 105.0 kHz VISCOSITY: 2.81 cP

AMPLITUDE - volts	TIME - µs	SEPARATION - cm
0.1190	60.41	6.04
0.0846	70.00	8.03
0.0640	79.91	10.05
0.0505	89.64	12.02
0.0408	99.09	14.01
0.0340	108.63	16.00
0.0282	119.06	18.06
0.0245	126.97	19.96

VELOCITY: 2074.5 m/s

STANDARD DEVIATION OF VELOCITY: 13.0 m/s

LINEAR CORRELATION COEFFICIENT: 0.9999

ATTENUATION: 2.80 Np/m

STANDARD DEVIATION OF ATTENUATION: 0.16 Np/m

BEAD TYPE: MS-MH

FREQUENCY: 105.0 kHz VISCOSITY: 3.23 cP

AMPLITUDE - volts	TIME - µs	SEPARATION - cm
0.1160	60.36	6.07
0.0830	69.85	8.06
0.0640	79.20	10.06
0.0505	88.30	12.01
0.0410	98.12	14.03
0.0336	107.62	16.02
0.0280	117.86	18.01
0.0240	126.48	20.05

VELOCITY: 2089.8 m/s

STANDARD DEVIATION OF VELOCITY: 12.1 m/s

LINEAR CORRELATION COEFFICIENT: 0.9999

ATTENUATION: 2.80 Np/m

STANDARD DEVIATION OF ATTENUATION: 0.26 Np/m

BEAD TYPE: MS-MH

FREQUENCY: 105.0 kHz VISCOSITY: 2.46 cP

AMPLITUDE - volts	TIME - µs	SEPARATION - cm
0.1158	61.06	6.07
0.0820	71.26	8.09
0.0616	80.76	10.07
0.0484	90.82	12.06
0.0.396	100.46	14.03
0.0328	110.37	16.02
0.0274	119.43	18.01
0.0231	129.68	19.98

VELOCITY: 2034.7 m/s

STANDARD DEVIATION OF VELOCITY: 8.2 m/s

LINEAR CORRELATION COEFFICIENT: 1.0000

ATTENUATION: 2.99 Np/m

STANDARD DEVIATION OF ATTENUATION: 0.19 Np/m

BEAD TYPE: MS-MH

FREQUENCY: 105.0 kHz VISCOSITY: 2.09 cP

AMPLITUDE - volts	TIME - µs	SEPARATION - cm
0.1210	61.73	6.01
0.0870	71.80	8.02
0.0660	82.32	10.06
0.0526	91.83	12.02
0.0429	101.86	14.00
0.0355	112.19	16.02
0.0302	122.23	18.02
0.0262	132.08	19.99

VELOCITY: 1986.6 m/s

STANDARD DEVIATION OF VELOCITY: 3.6 m/s

LINEAR CORRELATION COEFFICIENT: 1.0000

ATTENUATION: 2.39 Np/m

STANDARD DEVIATION OF ATTENUATION: 0.19 Np/m

REFERENCES

Bedford, A., G. Ellis, K. P. Elliot, S. K. Mitchell, D. J. Shirley, "Acoustical Properties of Sediments," Applied Research Laboratories Technical Report No. 82-47 (ARL-TR-82-47), Applied Research Laboratories, The University of Texas at Austin (1982).

Bedford, A., R. D. Costley, and M. Stern, "On the Drag and Virtual Mass Coefficients in Biot's Equations," J. Acoust. Soc. Am. 76, 1804-1809 (1984).

Bell, David W., "Shear Wave Propagation in Unconsolidated Fluid Saturated Porous Media," Applied Research Laboratories Technical Report No. 79-31 (ARL-TR-79-31), Applied Research Laboratories, The University of Texas at Austin (1979).

Bevington, Philip R., "Data Reduction and Error Analysis for the Physical Sciences" (McGraw-Hill, Book Co., Inc., New York, 1969).

Biot, M. A., "Theory of Propagation of Elastic Waves in a Fluid-Saturated Porous Solid. I. Low Frequency Range," J. Acoust. Soc. Am. 28, 168-178 (1956a).

Biot, M. A., "Theory of Propagation of Elastic Waves in a Fluid-Saturated Porous Solid. II. Higher Frequency Range," J. Acoust. Soc. Am 28, 179-191 (1956b).

Biot, M. A., " Generalized Theory of Acoustic Propagation in Porous Dissipative Media," J. Acoust. Soc. Am. 34, 1254-1264 (1956c).

Blackstock, David T., Notes from "Acoustics I and II," courses given in the Departments of Mechanical Engineering and Electrical Engineering at The University of Texas at Austin.

Greenspan, Martin, "Acoustic Properties of Liquids," in American Institute of Physics Handbook, 3rd ed., Dwight E. Gray, ed. (McGraw-Hill Book Co., Inc., New York, 1963), pp. 3-79.

Hovem, J. M., and G. D. Ingram, "Viscous Attenuation of Sound in Saturated Sand," J. Acoust. Soc. Am. 66, 1807-1811 (1979).

Kinsler, L. E., A. R. Frey, A. B. Coppens, and J. V. Sanders, Fundamentals of Acoustics, 3rd ed. (John Wiley & Sons, Inc., New York, 1982), p. 461.

Sheely, Madison L., Industrial and Engineering Chemistry 24, 1060-64 (1932).

Shirley, Donald J., and David W.Bell, "Acoustics of in Situ and Laboratory Sediments," Applied Research Laboratories Technical Report No. 78-36 (ARL-TR-78-36), Applied Research Laboratories, The University of Texas at Austin (1978).

Stoll, R. D., "Acoustic Waves in Saturated Sediments," in Physics of Sound in Marine Sediments, L. D. Hampton , ed. (Plenum Press, New York, 1974), pp. 19-39.

Stoll, R. D., "Acoustic Waves in Ocean Sediments," Geophysics 42, 715-725 (1977).

ACKNOWLEDGMENTS

The author was fortunate to receive contributions and support from several persons. Dr. A. Bedford supervised this research and was an appreciated source of encouragement and patience. Dr. Paul Vidmar made many contributions and suggestions.

Dr. Ilene Busch-Vishniac answered my many questions, particularly those involving the design of the transducers and error analysis. The transducer design was primarily the result of two conversations with Dr. Elmer Hixson. Mr. Ken Kirksey made several contributions in the development of the transducers, particularly in their construction. Dr. David Blackstock was very encouraging and referred me to several helpful sources. I was also fortunate to visit Mr. James Matthews' lab at NORDA and to witness some of the progress he has made in experimental sediment acoustics. Dr. George B. Thurston advised me on the viscosity measurements. I am indebted to Mr. Donald J. Shirley and Mr. Kenneth P. Elliot, who both preceded me in the sediments lab at ARL:UT. The experiment was the brain child of Mr. Shirley.

Ms. Jo Lindberg and Mr. James TenCate made several contributions concerning instrumentation.

This research was supported by the Office of Naval Research, Code 425GG and Code 400, and was submitted to the Graduate School of The University of Texas at Austin in partial fulfillment of the requirements for the degree of Master of Science in Engineering.

May 1985

DISTRIBUTION LIST FOR
ARL-TR-85-14
UNDER CONTRACT N00014-80-C-0490

Copy No.

Office of Naval Research
495 Summer Street
Boston, MA 02210
1 Attn: R. L. Sternberg

Commanding Officer
Naval Ocean Research and Development Activity
NSTL Station, MS 39529
2 Attn: E. D. Chaika (Code 530)
3 D. B. King (Code 321)
4 R. Wagstaff (Code 245)
5 K. Gilbert (Code 221)
6 A. Wenzel
7 G. Morris (Code 425GG)
8 J. Matthews (Code 362)

Chief of Naval Research
Department of the Navy
Arlington, VA 22217
9 Attn: M. McKisic (Code 425-OA)
10 R. Obrochta (Code 425-AR)
11 F. E. Saalfield (Code 400)

Director
Naval Research Laboratory
Department of the Navy
Washington, DC 20375
12 Attn: O. Diachok (Code 5128)
13 R. Dicus (Code 5128)
14 R. Gragg

Lawrence Livermore National Laboratory
P. O. Box 808, L-200
Livermore, CA 94550
15 Attn: J. G. Berryman

Planning Systems, Inc.
7900 Westpark Drive
Suite 600
McLean, VA 22102
16 Attn: B. Brunson

Distribution List for ARL-TR-85-14 under Contract N00014-80-C-0490 (cont'd)

Copy No.

	Lamont-Daherty Geological Observatory Columbia University Palisades, NY 10964
17	Attn: R. D. Stoll
18	A. Mark Bedford, ARL:UT
19	H. Boehme, ARL:UT
20	Ilene J. Busch-Vishniac, ARL:UT
21	Karl C. Focke, ARL:UT
22	Thomas A. Griffy, ARL:UT
23	John M. Huckabay, ARL:UT
24	Robert A. Koch, ARL:UT
25	Stephen K. Mitchell, ARL:UT
26	T. G. Muir, ARL:UT
27	David W. Oakley, ARL:UT
28	Clark S. Penrod, ARL:UT
29	Morris Stern, ARL:UT
30	James A. TenCate, ARL:UT
31	Paul J. Vidmar, ARL:UT
32	Gary R. Wilson, ARL:UT
33	H. Yew, ARL:UT
34	Library, ARL:UT